A&A 443, 41–60 (2005)
DOI: 10.1051/0004-6361:20052908

Astronomy & Astrophysics

Star-formation in NGC 4038/4039 from broad and narrow band photometry: cluster destruction?⋆,⋆⋆

S. Mengel[1], M. D. Lehnert[2], N. Thatte[3], and R. Genzel[2,4]

[1] European Southern Observatory, Karl-Schwarzschild-Str. 2, 85748 Garching, Germany
e-mail: smengel@eso.org
[2] Max-Planck-Institut für extraterrestrische Physik, Giessenbachstraße, 85748 Garching, Germany
e-mail: mlehnert@mpe.mpg.de
[3] University of Oxford, Dept. of Astrophysics, Denys Wilkinson Building, Keble Road, GB-Oxford OX1 3RH, UK
e-mail: thatte@astro.ox.ac.uk
[4] Also at Department of Physics, University of California at Berkeley, 366 Le Conte Hall, Berkeley, CA 94720-7300, USA
e-mail: genzel@mpe.mpg.de

Received 19 February 2005 / Accepted 18 May 2005

ABSTRACT

Accurately determining the star formation history in NGC 4038/4039 – "The Antennae" – is hampered by variable and sometimes substantial extinction. We therefore used near infrared broad- and narrow-band images obtained with ISAAC at the VLT and with SOFI at the NTT to determine the recent star formation history in this prototypical merger. In combination with archival HST data, we determined ages, extinction, and other parameters for single star clusters, and properties of the cluster population as a whole.
About 70% of the K_s-band detected star clusters with masses $\geq 10^5$ $M_\odot$ are younger than 10 Myr (this is approximately an e-folding time for cluster ages), which we interpret as evidence of rapid dissolution but not free expansion.
The total mass of K-band selected clusters is about 5 to 10×10^8 $M_\odot$ and represents about 3–6% of the total molecular gas. However, this takes only the detected clusters into account, and in view of the rapid dissolution, means that this is only a lower limit to the total mass of stars produced in clusters during the burst. Studies of cluster formation in other galaxies recently suggested short cluster dissolution timescales, too, which means that star formation rates may have been severely underestimated in the past.
Extinction is strongly variable and very high in some regions, but around $A_V = 1.3$ mag on average. Even though most clusters are detected at least in I-band, only the information about individual cluster ages and extinction allows us to avoid uncertainties of orders of magnitude in star formation rate estimates determined from optical fluxes. From the distribution of individual cluster extinction vs. age, which is significantly higher for clusters below 8–9 Myr than for older clusters, we infer that this is the time by which a typical cluster blows free of its native dust cocoon.

Key words. galaxies: star clusters – galaxies: individual: NGC 4038/4039 – galaxies: interactions

1. Introduction

NGC 4038/4039 – "the Antennae" – is one of the closest ($D \sim 19.3$ Mpc, $H_0 = 75$ km s^{-1} Mpc^{-1}) examples of merging spiral galaxies and thus has been the target of detailed studies in many wavelength ranges (e.g., Whitmore et al. 1999; Fabbiano 2001; Wilson et al. 2001, etc.), some aimed at unveiling the star formation properties. However, the term "unveil" is appropriate also in a literal sense, since many of the active star formation sites – especially in the region where the two galaxies seem to overlap (therefore often referred to as "overlap region") are hidden by up to several optical magnitudes of extinction. Mid- and far infrared wavelengths are essentially not affected by this, but the spatial resolution of the images is too low to resolve the star formation regions into single star clusters. We therefore aimed at a compromise by observing the merger in the near infrared, where the extinction is only ∼10% of that at visible wavelengths, but where ground-based telescopes currently deliver sub-arcsecond resolution if atmospheric conditions are favourable. We combine the information from these broad band (Ks, ISAAC on the ESO-VLT) and narrow band

⋆ Based on observations collected at the European Southern Observatory, Chile, programme identification numbers 63.N-0528, 65.N-0577, and 67.B-0504.

⋆⋆ Data table for 1072 K-band detected clusters is only available in electronic form at the CDS via anonymous ftp to cdsarc.u-strasbg.fr (130.79.128.5) or via http://cdsweb.u-strasbg.fr/cgi-bin/qcat?J/A+A/443/41

(CO 2.34 μm, ISAAC and Brγ, SOFI on the ESO-NTT) images with archival Hubble Space Telescope WFPC2 images (broad-bands roughly corresponding to U, B, V, I, and narrow band Hα, see Whitmore et al. 1999, hereafter W99) for our investigation of the properties of the numerous compact star clusters in the Antennae.

What we determined from these data are a number of properties of the single star clusters, namely their ages, the extinction towards them, and their photometric masses. Additionally, we derived properties of the ensemble of star clusters as a whole: the age distribution over the last ≈200 Myr (including the mass production in the burst), the average extinction for cluster populations of different ages, and various other estimates. This analysis is complemented by an estimate of the bias introduced by using only the Ks-band detected clusters, be it an age or mass selection effect.

2. Observations and data reduction

ISAAC (VLT-ANTU) imaging of NGC 4038/4039 was performed in ON/OFF mode during the nights 15.04.2001 (Ks-band) and 16.04.2001 (CO-band-head filter). The target fit completely onto the detector (0.″1484/pixel, total field size 2.′5 × 2.′5). Seeing was excellent during both of these photometric nights (PSF *FWHM* of the co-added frames is below 0.″4), and the total on-source time was 360 s (Ks) and 480 s (CO), respectively. No narrow band continuum observations were performed; therefore, the Ks-image was used for continuum subtraction.

SOFI (NTT) imaging during 11./12.05.99 covered all NIR broad- and several narrow bands, however, seeing was much worse than for the ISAAC data (between 0.″6 and 1.″2 PSF *FWHM*), so that only the 0.″7 Brγ-data will be used for the analysis. Here the field size was roughly twice that of ISAAC (4.′9 × 4.′9, with a pixel size of 0.″292). Therefore, to save observing time, an on-chip offset pattern was observed instead of the usual ON/OFF mode. Due to a slight haze, conditions were not photometric on either of the nights. Table 1 lists descriptions of the observations analysed in this paper for both, the ISAAC and the SOFI runs.

Reduction of the ISAAC data was performed using the IRAF package[1]. It included dark and sky subtraction either using the median of several neighbouring sky images (or, where this led to residuals, doing pairwise subtraction), and flat fielding by a normalized median of all sky frames. All of the ON frames were slightly offset with respect to each other, in order to minimize the effect of pixel defects. Therefore, they had to be shifted to a common location before using the *imcombine* task, setting the minmax rejection algorithm to reject the highest and the lowest pixel, to combine the single frames. A photometric standard (GSPC S279-F, Ks-magnitude 12.031) was used for flux calibration (the resulting zero-point was 24.28 mag). The data reduction procedure for the CO narrow band images was identical.

[1] IRAF is distributed by the National Optical Astronomy Observatories, which are operated by the Association of Universities for Research in Astronomy, Inc., under cooperative agreement with the National Science Foundation.

Table 1. Summary of the NTT-SOFI and VLT-ISAAC NIR imaging observations.

Band	$\lambda_{\rm cen}$ [μm]	Width [μm]	DIT [s]	Total ON [s]	Seeing *FWHM*
Ks	2.16	0.27	6	360	0.″4
Brγ	2.167	0.028	30	1500	0.″7
$CO_{2.34}$	2.34	0.030	60	480	0.″4

The resulting Ks-band frame is displayed in Fig. 1, with circles indicating the point-like sources that were detected using *daofind* from the *DAOPHOT* package. A detection threshold of 3σ was chosen, leading to 1072 detected objects, which are marked in that figure.

Reduction of the SOFI data essentially followed the same procedure, with the two differences: 1) there were no real OFF frames, therefore several images with observing times closest to the currently treated frame were medianed for sky subtraction; 2) due to a wrong setting of the "Pupil Rotation" switch, the object orientation varied from frame to frame, especially during the transit of the object. This had to be accounted for before the co-addition of the frames. They were rotated by the angle derived from the header information.

HST WFPC2 images were reduced using the IRAF *stsdas.hst_calib.wfpc* package, and photometric calibration used the zero-points and colour transformations given in Holtzman et al. (1995) in their Table 7 and Eq. (8). For Hα, we set the zero-point to reproduce the magnitudes of several stars and clusters lacking Hα emission, which we know from our 3D Mengel et al. (2001) and ISAAC spectroscopy Mengel et al. (2002) data, for a linear interpolation between V and I magnitudes at the central wavelength of the Hα filter (18.316 mag).

However, in order to be able to combine the optical and the near-infrared data sets, we binned the WFPC2 images down to the pixel size of the ISAAC frame and rotated them to match orientation. Therefore, in the following, whenever the unit "pix" is used, it refers to the ISAAC Hawaii array imaging scale of 0.″148/pix.

Photometry was then performed on the target list, which was created using the Ks-band image. Running *daofind* on the V-band image results in more than 10 000 detected point-like sources. However, the analysis of the HST data alone was thoroughly performed by W99. Since we are interested in the additional information brought about by the K-band data, we restrict our analysis to those objects which are detected in Ks.

In order to estimate the total cluster magnitudes required for the mass estimates of the clusters, and also in order to obtain colours combining the optical and near infrared bands, we used a curve of growth technique to estimate the magnitudes of relatively isolated clusters (distance to nearest cluster more than 10 (12) pixels in V (Ks)-band). We assigned the magnitude at a radius where the magnitude no longer changed significantly. For a number of those clusters we determined aperture corrections for both bands and applied these to the clusters in the more crowded regions, where cluster distances were below the mentioned limits. Due to the different PSF *FWHM*s in the

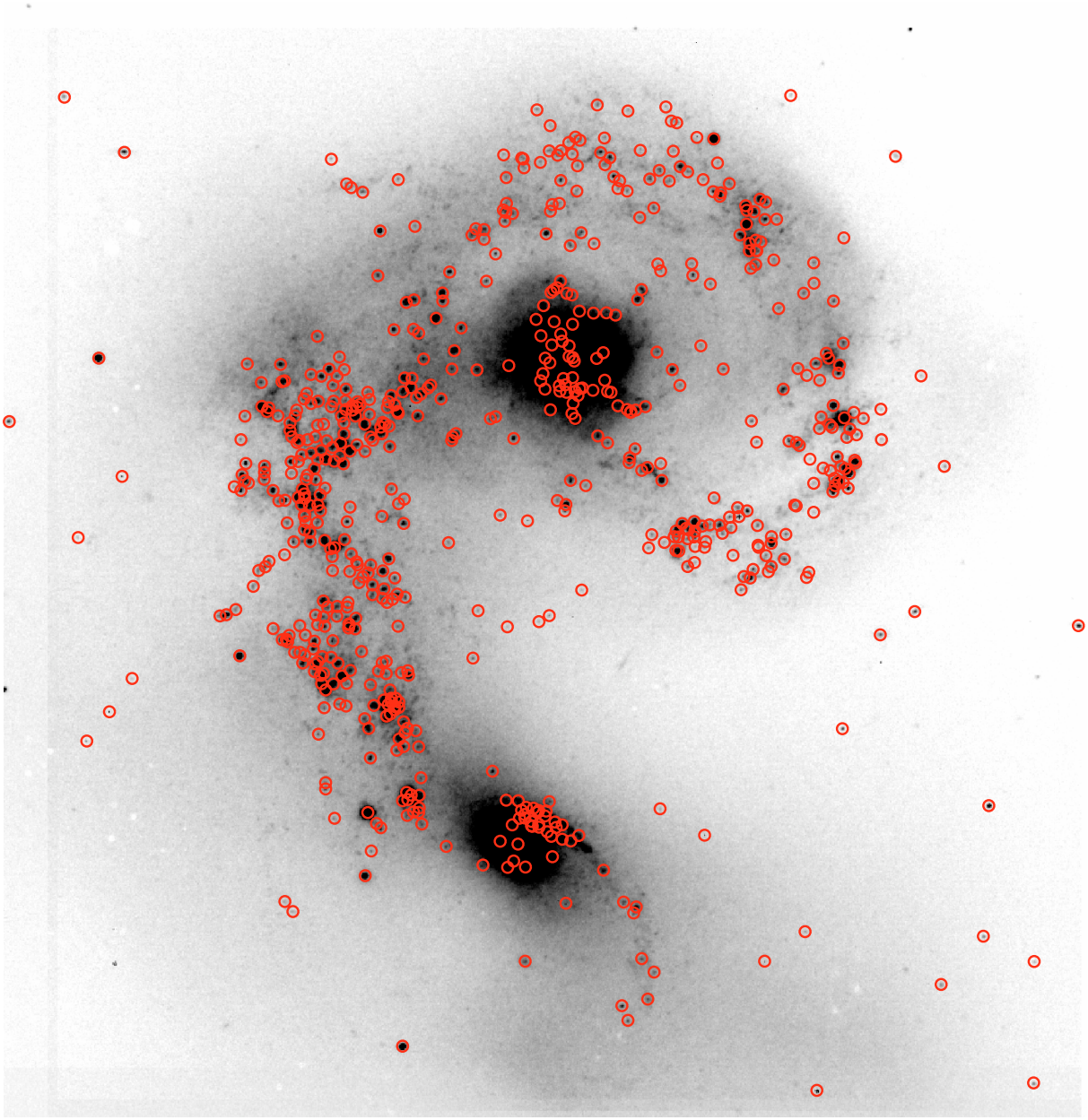

Fig. 1. *K*s-band ISAAC image with the location of the 1072 detected point-like sources marked. *FWHM* of the PSF in this image is below 0.″4. Not all of the detected sources are clusters, as there are also a few foreground stars and background galaxies.

two bands (V: 1.6 pix, Ks: 2.6 pix), we used different fixed apertures (V: r = 3 pix, Ks: r = 5 pix), and the aperture corrections were 0.7 mag and 0.5 mag for V and Ks, respectively. So, in summary, for the isolated clusters we used the curve-of-growth technique, and therefore variable apertures, to obtain the total magnitudes, whereas for clusters with nearby neighbours, we performed aperture photometry and applied an average aperture correction. We then determined optical colours ($U-B$, $B-V$, $V-I$) all within the same apertures (r = 3 pix), since the PSF did not vary significantly over the optical wavelength range.

For the computation of Hα fluxes, we used the magnitudes of the Hα photometry within the r = 3 pix aperture and subtracted a continuum flux estimated from a linear interpolation of the V- and I-band fluxes at the central wavelength of the used narrow band filter ($\lambda_{\rm cen}$ = 658 nm). We decided to take such a small aperture to avoid including flux from neighbouring clusters in the cases of crowded regions. Radial plots performed on some of the isolated, bright clusters in the continuum-subtracted Hα image showed us that most (70%−95%) of the emission line flux was indeed contained within this aperture. However, in the crowded regions with many clusters around 7 Myr, overlap in the emission line flux is quite common (see the red channel of Fig. 4 in Whitmore et al. 1999). The largest shells of some older clusters have radii of more than 20 pixels, and we clearly cannot integrate out to these distances without including a lot of neighbouring clusters. Our selection of a 3 pix radius is therefore the attempt to optimize the result for young clusters with strong emission. For older clusters with extended, low-luminosity shells, this will

lead to age estimates which are too old, but we will only use the information from the Hα emission for strong Hα emitters, anyhow.

Brγ-fluxes were more difficult to obtain, due to the much lower spatial resolution. Here we proceeded as follows. We first convolved the *K*s-band image with a Gaussian, so that the PSF *FWHM* matched that of the Brγ image. Then we performed photometry on both images (the zero-point of the Brγ image set such that the *K*-band magnitudes of stars and clusters known to lack Brγ emission[2] were reproduced) for the 1072 point source positions detected in the higher resolution image. We then used the *K*s-band fluxes as the continuum fluxes, and determined Brγ fluxes and equivalent widths from the difference of the two images. In the locations of extremely strong Brγ emission (equivalent width above 150 Å), the Brγ flux is likely to be underestimated by 5−7%, due to the line contribution to the continuum filter.

CO (2.34 μm) images had the same PSF *FWHM* as the *K*-band images; therefore, the procedure was facilitated here compared to the SOFI narrow band data. We set the zero-point of the image to reproduce the magnitudes of stars and isolated clusters known to lack CO band-head absorption[2] (Z = 21.475 mag). The CO index is created taking the ratio of the flux in the CO narrow band filter with that in the *K*s-band filter and expressing it in magnitudes. Using the broad-band filter for an estimate of the continuum should be fine, because it cuts off just short of the rest wavelength of the first CO band-head (also see Fig. 3). Only in cases of extremely high Brγ equivalent widths (above 150 Å), a CO index of up to 0.07 mag can be obtained despite the absence of CO absorption. The aperture used for determination of the CO index was 5 pix.

3. Analysis and results

We used several different approaches to estimate the ages and extinction in individual clusters based on broad- and narrow-band photometry; we are only talking about "clusters", because even the brightest supergiants with $M_K = -12$ mag are unfortunately still below our detection limit. Subsequently, these methods were combined to yield the cluster properties. Broad-band photometry was used to simultaneously estimate cluster age and extinction by fitting the (usually) five data points to colours from a Starburst99 (Leitherer et al. 1999) model for ages up to 500 Myr.

In order to be able to compare our photometry with the predictions of Starburst99, we applied three corrections to the models:

- In *V*-band and *K*s-band, we accounted for line emission included in the filter bandpass.
- The filter systems onboard HST do not exactly match the assumed filter transmission in the Starburst99 code, but differences are only significant for *I*-band. We therefore transformed the theoretical *I*-magnitudes to the HST photometric system.
- The CO index computed by Starburst99 is a spectroscopic index that does not exactly correspond to the index that results from our choice of filters, so we derived a new analytic expression for the variation of CO index with effective temperature and inserted this in the Starburst99 code.

The following subsections explain the procedures we followed in detail:

3.1. V-band and Ks-band: inclusion of line emission

The HST broadband filter that most closely resembles the Johnson *V*-band filter is *F555W*, and the zero-points and transformations described in Sect. 2 actually convert the magnitudes to the Johnson system. The transmitting wavelength range of this filter includes several emission lines, amongst them Hα and Hβ,

We made a crude attempt to take this line emission into account in the theoretical predictions of the Starburst99 code. The Hβ line will contribute the largest amount of hydrogen recombination line emission, because at the position of the Hα line (6563 Å), the filter transmission is already down to the ≈10% level, while the intrinsically fainter Hβ line (4861.33 Å) lies in the region of highest transmission (≈90%). Also the [OIII] line lies in the region of high transmission; and even though its strength depends on environmental parameters, it is typically much stronger than Hβ. We included its contribution by using the "typical Galactic HII-region" line ratios listed in Anders & Fritze-v. Alvensleben (2003), amounting to a factor of 5.5. To determine the absolute line fluxes we used the *V*-band magnitudes and the Hα equivalent widths predicted by the Starburst99 code, while for the strength of the Hβ line we assumed the theoretical line ratio of Hα/Hβ of 3.3 for Case B recombination (Osterbrock 1974). Modifications in the predictions of *V*-band magnitude are only noticeable for cluster ages younger than ≈6 Myr. In a similar way, Brγ emission was included in the *K*s-band filter predictions. However, the contribution is quite small. Only for clusters below 4 Myr, the difference in *K*s-magnitude amounts to more than 0.05 mag.

3.2. I-band photometry

While the HST filter set most closely resembles the Johnson-Cousins-system, which means that the *I*-band filter is in the Cousins system, the Starburst99 code assumed an *I*-band filter transmission curve corresponding to the Johnson system. In order to obtain a transformation between the two systems, we used photometry in both systems for stars of spectral types B2 to K4, taken from Landolt (1983) for the Cousins system and from Moffett & Barnes (1979) for the Johnson system. We converted the Starburst99 *I*-band magnitudes from the Johnson system to the Cousins system using the following expression:

$$I_{\rm Cousins} = I_{\rm Johnson} + 0.28 * (V - I)_{\rm Johnson-Cousins} - 0.01.$$

Figure 2 shows the data points we used together with this best fit.

[2] From our 3D (Mengel et al. 2001) and ISAAC spectroscopy (Mengel et al. 2002) data.

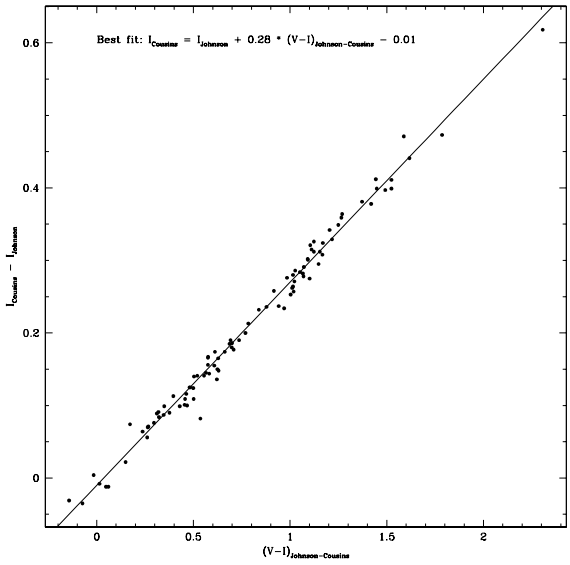

Fig. 2. $V-I$ colours in the Johnson-Cousins system and the difference between the Cousins and the Johnson I-band magnitudes plotted for stars of spectral types B2 to K4, taken from Moffett & Barnes (1979) and Landolt (1983). Over-plotted is the best fit to the data, which is represented by the given analytic expression.

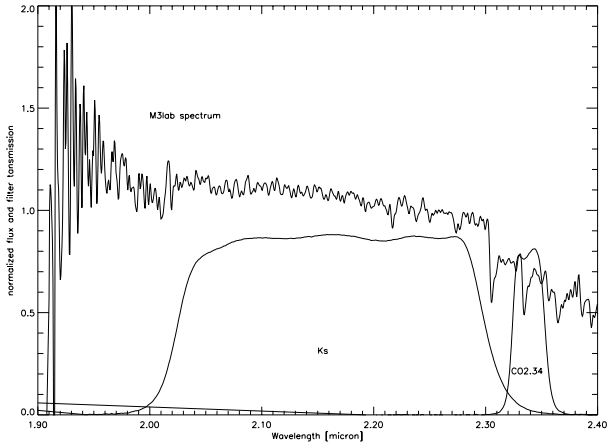

Fig. 3. Two curves which display the transmission of the $CO_{2.34}$ narrow band filter and of the Ks broadband filter installed at VLT-ISAAC. The spectrum is a red supergiant of spectral type M3Iab from the stellar library of Lançon & Wood (2000), which was shifted in wavelength appropriate to the redshift of the Antennae galaxies. Note that the Ks filter cuts off just short of the CO band-head and is not substantially influenced by its absorption.

3.3. CO index

As mentioned in Sect. 2, we used the narrow band $CO_{2.34}$ μm filter and the broadband Ks filter for estimating the CO index. This arrangement is a close approximation to the photometric CO index defined in Kleinmann & Hall (1986), who use another narrow band filter for an estimate of the K-band continuum. The spectroscopic CO index computed in Starburst99 is the spectroscopic CO index defined by Origlia & Oliva (2000). Rather than attempting a conversion, we used the giant and supergiant stars in the near infrared stellar library assembled by Lançon & Wood (2000). The K-band spectra of the stars were

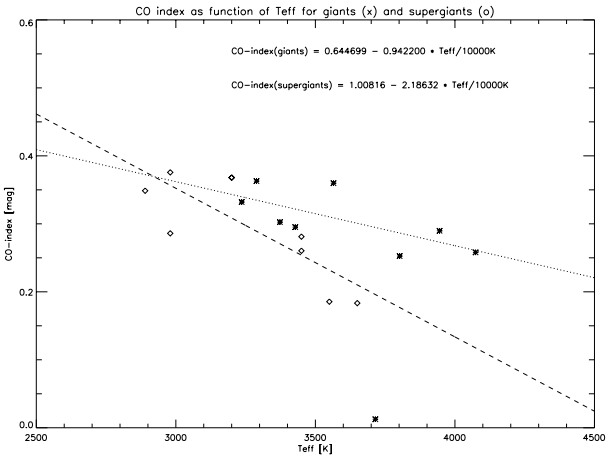

Fig. 4. The CO index as a function of effective temperature estimated for the redshifted spectra from the stellar library of Lançon & Wood (2000) using the ESO filter transmission curves from Fig. 3. The lines are the two best linear fits for supergiants and giants, respectively.

redshifted approximately to the redshift of the Antennae galaxies ($z \approx 0.005$), and we estimated their CO indices using the ESO filter transmission curves for the Ks and the $CO_{2.34}$ filter. From this analysis, we determined two analytic expressions for the CO index as a function of effective temperature, one for the giant and one for the supergiant stars. We did not determine the CO indices for dwarf stars, because at cluster ages below a few hundred million years, their contribution is negligible. We note that the library of Lançon & Wood (2000) only includes high luminosity stars, but had we expected a substantial contribution for our purposes, we would have included them using a different library.

The two analytic expressions we derived are:

$$\text{CO index} = 0.645 - 0.942 * \frac{T_{\rm eff}}{10\,000\ \rm K} \qquad \text{(giants)}$$

$$\text{CO index} = 1.008 - 2.186 * \frac{T_{\rm eff}}{10\,000\ \rm K} \qquad \text{(supergiants)}$$

and the data points and the corresponding fits are shown in Fig. 4.

We replaced the corresponding expressions (Doyon et al. 1994) in the Starburst99 code by these two expressions, then reran it to produce the evolution of the feature for an instantaneous burst at solar metallicity for an IMF with Salpeter slope between 1 and 100 $M_\odot$. The result is shown in Fig. 5. The general evolution of the feature is the same as for other age tracers using this spectral feature, like the above-mentioned photometric and spectroscopic indices, or the equivalent width. Only the absolute values have changed, and they can now be compared with our observations. See Sect. 3.5 for this comparison.

For six clusters, we have information about the equivalent width of the CO band-head (as defined in Origlia et al. 1998, and used in Starburst99) from spectroscopic or integral field spectroscopy data (see Mengel et al. 2001, 2002). We compare (see Table 2) these values and the corresponding age predictions to the CO index and assigned ages for two reasons: first, in order to check the reliability of the technique, and second,

Table 2. Comparison of ages derived from W_{CO} obtained from spectroscopy (3D at the AAT and ISAAC at the VLT) with our narrow-band-determined CO index. For definition of W_{CO}, CO index and extinction correction, please see text. The identification refers to the numbers used in Whitmore et al. (1999) and Whitmore & Schweizer (1995), respectively. [1] This value is completely off-scale, even if uncertainties are large. The age we assign is the range corresponding to the maximum CO index of ≈0.22.

Identification	A_V [mag]	W_{CO} [Å]	CO index (ext. corr) [mag]	Age (W_{CO}) [Myr]	Age (CO index) [Myr]
W99-1	0.094	17.5 ± 1	0.199	8.6...12.7	8.6...12.5
W99-2	0.03	16.2 ± 0.2	0.165	8.5 or 12.8	8.4 or 12.7
W99-15	1.02	17.0 ± 0.2	0.279	8.6...11.5	8.7...12.3
W99-16	≈0	19 ± 4	0.673[1]	8.2...12.9	8.7...12.3
WS95-355	2.88	16.3 ± 0.2	0.134	8.5 or 12.8	8.2 or 13
WS95-80	4.01	0	–0.02	≤7.3	≤7.3

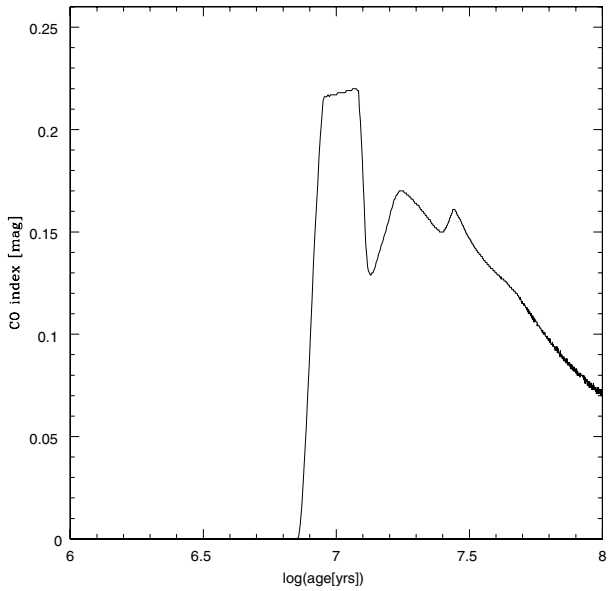

Fig. 5. The evolution of the CO index using the ESO $CO_{2.34}$ and *K*s filters, as it is predicted by Starburst99 after applying corrections for the definition of the index. The general behaviour is similar to other CO indices or equivalent widths definitions with only the absolute values differing.

to assess how strong the influence of extinction on the observed CO index is. We ended up extinction-correcting the CO index according to the following formula, which makes a noticeable difference only for clusters with an A_V of above ≈2 mag;

$$\text{CO index(extinction corrected)} = \text{CO index} + 0.012 * A_V.$$

This accounts for the differential extinction expected from the difference in central wavelength between the two filters. The two higher extinction clusters (W95-355 and W95-80) in Table 2 would allow for an even higher correction factor, but we stuck to this physically justified correction.

As can be seen from Table 2, the agreement is quite good for these clusters, but it is also obvious from the two clusters with high extinction that it improves agreement to apply an extinction correction for A_V above ≈2 mag. It is unfortunate for this purpose that our spectroscopic studies were heavily biased towards clusters around 10 Myr of age, because this narrows down the age range available for comparison between spectroscopy and narrow band imaging.

3.4. Our standard model

We used the Starburst99 (Leitherer et al. 1999) model, because it focuses on young stellar populations, which are dominant in this young merger. Nevertheless, we would have liked a model which also takes the thermally pulsing AGB phase into account, to be able to assess the impact they have on *K*-band luminosity. It is large according to some authors (see for example Förster-Schreiber et al. 2003, and references therein; and Schultz et al. 2002), but depends a lot on assumptions like the duration of that phase. Just before this paper was ready for submission, the new version of Starburst99 (Vazquez & Leitherer 2005, including the Padova tracks with full AGB evolution) became available; too late to re-do the analysis, but in time to add one track to Fig. 10. It shows that the impact on our interpretation would have been marginal, if we had used the new models instead. The 10 Myr (red supergiant) peak in *K*-band luminosity has a smaller amplitude and is somewhat wider in the new model, which would probably have caused our age distribution to get slightly wider. We emphasize, however, that the peak introduced by the population of TP-AGB stars of around 200 Myr is not pronounced enough to have shifted a significant fraction of the *K*-band selected clusters into that age range within our detection limit. Thus the differences in the models did not lead to a significant number of incorrect (younger) age assignments.

The characteristics of the model we used throughout this paper (unless noted otherwise) was an instantaneous burst with solar metallicity and a Salpeter IMF with a low and high mass cut-off of 1 and 100 $M_\odot$, respectively. These parameters are justifiable. The instantaneous burst is applicable because the star clusters are typically very small (effective radii of a few parsec) and very concentrated, which means that the star formation event is essentially instantaneous.

Solar metallicity or just slightly above is what we determined for a few bright individual clusters in the Antennae from an analysis of UVES high spectral resolution spectra (paper in preparation). Note that Vazquez & Leitherer (2005) caution against using their model (or any current evolutionary synthesis model) for stellar populations with sub-solar abundances and a

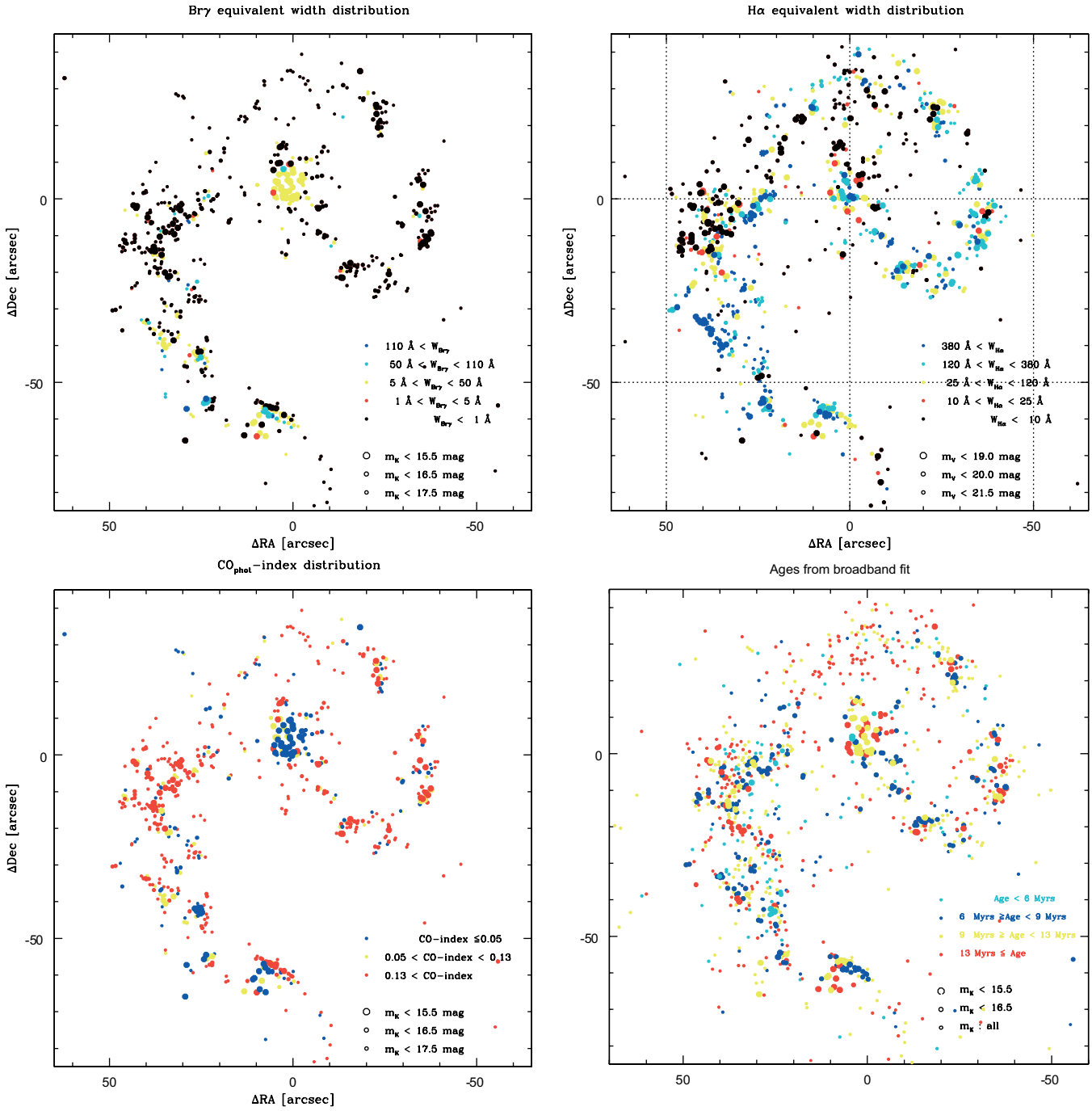

Fig. 6. Spatial distribution of the three narrow band age diagnostics with the colour coding as indicated in the individual plots. Generally, blue and cyan colours indicate younger clusters than magenta and red, but the legends for each plot should be consulted for individual comparisons. The general distributions of ages are very similar, and the ages determined from the various diagnostics coincide within a few Myr for most clusters. There are a few exceptions, however, where one or more of the indicators show a deviant value.

significant population of red supergiants. This is the main reason we decided to fix the metallicity at a reasonable average value, rather than making it a fit parameter, despite the necessary caution suggested by Anders et al. (2004).

The IMF is probably only *on average* around Salpeter (Mengel et al. 2002), and we expect it to vary for the whole cluster population in a similar manner to what was seen for the subsample analysed in Mengel et al. (2002). Since we have not yet found a parameter which correlates significantly with IMF slope or lower mass cutoff, we assume this average value as determined by Mengel et al. (2002). Note that assuming, for example, a lower mass cutoff of 0.1 $M_\odot$ for the Salpeter IMF, or a Kroupa IMF (Kroupa 2001) instead, does not change our conclusions derived from relative quantities like colours or equivalent widths, because those IMFs largely add mass in the form of low-mass stars, which do not contribute a significant

amount of light at young ages. Only the cluster mass derived from the photometry would be higher than the ones we obtain, therefore our masses represent lower limits. For example, the mass of a cluster for a Salpeter IMF between 0.1 and 100 $M_\odot$ is higher by a factor 2.6.

3.5. Age determination

Our data set includes a number of age indicators, therefore we used the following strategy to assign individual ages to the *K*s-band detected clusters. We deemed this necessary (rather than a simple averaging of all available ages) because of the on/off nature of the narrow band diagnostics: for example, absence of CO absorption in a sufficiently bright cluster constrains the age to be anything below 6.3 Myr, which can be used to verify ages from other diagnostics, but not for straight averaging. In essence, what we did was:

- Firstly, we have the broadband data covering *U*, *B*, *V*, *I*, and *K*s, that should be suitable to age-date clusters of all ages. The large wavelength coverage, especially the inclusion of *K*s-band photometry, is suitable for breaking the age-extinction-degeneracy – see also Anders et al. (2004) for a more general discussion.
- Secondly, we can use narrow band emission line images: Hα and Brγ. The presence of hydrogen recombination line emission indicates a very young age of the cluster, below $\approx$7 Myr, and we use the equivalent width to determine the age if it is below this limit.
- Thirdly, CO band-head absorption narrow band images, where the detected spectral feature reveals the presence of red supergiants or giants, and is most efficient in identifying star clusters around 10 Myr of age.

As mentioned, we used the broadband data to break the degeneracy in age and extinction. To do that, we performed a simultaneous fit of the theoretical spectra for ages up to 500 Myr to the observed broadband magnitudes. The amount of extinction was determined by reddening the theoretical spectrum according to the Mathis (1990) extinction law. Note that we are assuming a foreground screen extinction. We believe this to be appropriate, because after the onset of stellar winds and supernovae, remnant gas and dust are expected to be driven out of the cluster within less than a crossing time (see Boily & Kroupa 2003), which for the clusters we have studied is $\lesssim 10^5$ yr. This material forms a cocoon around the cluster, which can be described as a foreground screen. A mixed model would have to be assumed if we analyzed the average extinction in the galaxy from integrated emission, but not in determining the extinction towards individual clusters. To simultaneously determine age and extinction, we used a simplex algorithm to tour data space, with a χ^2 minimization technique to find the best fitting pair of extinction/age.

Ages and extinction so obtained for the brighter clusters (only for brighter clusters, because the narrow band images were shallower) were complemented by extinction estimates derived from the ratio of Hα/Brγ flux compared to the value expected for a Case B recombination scenario, and by age estimates from the Brγ equivalent width, the Hα equivalent width, and the CO index.

The average ages were usually assigned by averaging the available data, but we kept track of the number of available data points and their level of agreement by assigning an "age quality" parameter, which is highest, if all four indicators (broadband fit, $W_{\mathrm{H}\alpha}$, $W_{\mathrm{Br}\gamma}$, CO index) are present and agree, and is lower for fewer data points or disagreement:

- If all four indicators yielded ages (74 cases), the common age was the average of the four, if the age difference between any of them was smaller than 4 Myr. The "age quality" was set to 4. If only three indicators agreed, their average was used and the fourth value ignored, with the quality value set to 3. If two or more ages were discrepant with respect to the others, the common age was set to the average of the Hα- and the Brγ-age, but the quality-value was set to a low value of 2.
- Similar strategies were followed for average age determinations if fewer than four indicators were available (three: 376, two: 320, one: 262), essentially averaging the available ages and assigning data quality parameters depending on the level of agreement. What should be mentioned is that for the cases where only one age was available (that would usually be the value from the broadband fit), that age was also assumed for the average age; those cases where only one or two indicators were available, but where the other indicators were expected to be missing, were also assigned high age quality parameters. For example, a cluster with an age determined to be older than 10 Myr from the broadband fit and the CO index is not expected to show Hα or Brγ. Therefore, it is assigned an age quality parameter of 3.9.

Out of our 1072 *K*s-band detected clusters, 40 could not be assigned any ages, 997 had ages from the broadband fit, 590 from the CO index, 128 from $W_{\mathrm{Br}\gamma}$, and 494 from $W_{\mathrm{H}\alpha}$. In general, the agreement between the age indicators was good: excellent agreement was seen for $\approx$340 clusters, another $\approx$500 showed good agreement, and only $\approx$230 were vastly discrepant, including the 40 clusters without an age determination. Their distribution is shown in Fig. 8. Most of the brighter ones of these objects with faulty age determinations were either foreground stars or located in the nuclear regions, which suggests that for the latter the high and variable background of the nucleus might be responsible for photometric errors that led to wrong age assignments – for example because line emission was erroneously detected or subtracted from the source because it is too extended. The fainter objects were distributed throughout the merger, which means that a disagreement in age determinations for them is probably caused by statistical uncertainties in the photometry. A 2-dimensional Kolmogorov-Smirnov test indicates that the spatial distribution of these clusters is marginally different from the distribution of all clusters (probability of 4.6%). This is because the clusters that lie in regions of high background relative to their total brightnesses are more likely to have discrepant ages than the general population of clusters. Thus bright bright clusters in the nuclei, for example, tend to have inconsistent age determinations, whereas

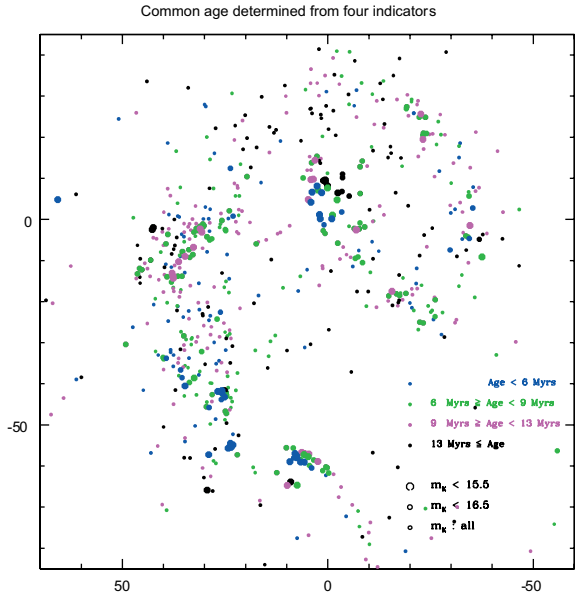

Fig. 7. Clusters with ages determined from all indicators. Only those with good agreement are shown. The median age is 9.2 Myr.

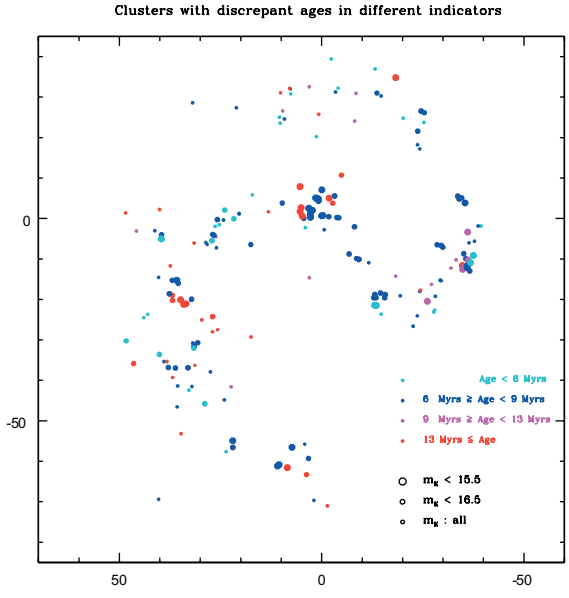

Fig. 8. Colour (age) and size (luminosity) distribution of clusters that had discrepant age determinations. Roughly 180 clusters fall into this category. The colour coding represents the best age fit determined from using only broad-band colours.

faint clusters with discrepant age determinations tend to be distributed more like the general population of clusters. This hypothesis is confirmed by running 2-dimensional K-S tests separately on the bright and faint sub-populations with discrepant ages compared to the general population of bright and faint clusters respectively. The dividing magnitude was chosen to be $m_K = 15.5$. For the following analyses, clusters with an "age quality" parameter below 3.0 were not taken into account, which means that foreground stars with their bad age fit are automatically excluded from the analysis.

The age distribution (see Figs. 7 and 9) shows two peaks, one at approximately 5−6 Myr, and one around 10 Myr. Older clusters are rare: there are two more peaks at around 28 and 200 Myr, with roughly 20 members each. The strong peak around 10 Myr is a selection effect which arises from the very high total *K*s-band luminosity around that age, leading to detection of large numbers of low mass (between 10^3 and a few times 10^4 $M_\odot$) clusters, which are below the detection limit at other ages.

However, one interesting aspect of the age distribution is that the relative numbers of 6 vs. 10 Myr old clusters shifts with limiting magnitude: going to brighter clusters, the younger ones become more dominant. This is expected from the luminosity evolution in *V*-band, where the youngest clusters are the brightest (see Figs. 47b and 51b in Leitherer et al. 1999, or Fig. 10 in this work for the luminosity evolution in *V* and *K*), but the absolute *K*s-band magnitude peaks at a cluster age of ≈10 Myr, where the luminosity contribution from the supergiants dominates that band. Therefore, we expected to see this trend in the plot of the *V*-band selected clusters (Fig. 9, top), but were surprised to also see this for the *K*s-band selected clusters (Fig. 9, bottom), even though to a lesser extent. Since we used the extinction corrected magnitudes, it is not extinction which causes this effect. It actually means that more high luminosity (and therefore high mass) clusters are present at ages around 6 Myr, compared to those around 10 Myr. This conclusion is also supported by Fig. 11, which clearly shows the drop in cluster numbers between 4 and 15 Myr for the high mass clusters. We performed a one-dimensional Kolmogorov-Smirnov (K-S) test in order to assess the significance of the decrease in cluster numbers. For the clusters above 10^5 $M_\odot$, we created many hundreds of random comparison populations, one assuming a constant probability in time, the other assuming an exponential probability distribution, both with the same total number of clusters as observed. In neither case did we concretely account for a selection function because as we have shown earlier, our selection should be robust for clusters with masses above 10^5 $M_\odot$ and ages <30−100 Myr. The probability that the observed population was drawn from a parent population with a constant distribution of cluster numbers in time is virtually zero (only 3.5%). The population is not consistent with being a simple exponential either – only a probability of 56%. For the clusters above 10^5 $M_\odot$, the only simple robust conclusion we can draw without conjuring up more complex models, is that the distribution of cluster ages is consistent with our visual impression, which is the number of clusters is declining significantly with age.

3.6. Extinction

A similar procedure to the one for the ages was followed determining the extinction A_V, assuming foreground screen extinction (see Sect. 3.5). For most clusters, it was determined from broadband colours, using the fitting routine described in Sect. 3.5 for a Mathis (1990) extinction law, but for those with $m_K < 17.3$ mag and $W_{\mathrm{Br}\gamma} > 80$ Å, the value determined from the observed flux ratios of Hα and Brγ was averaged with the

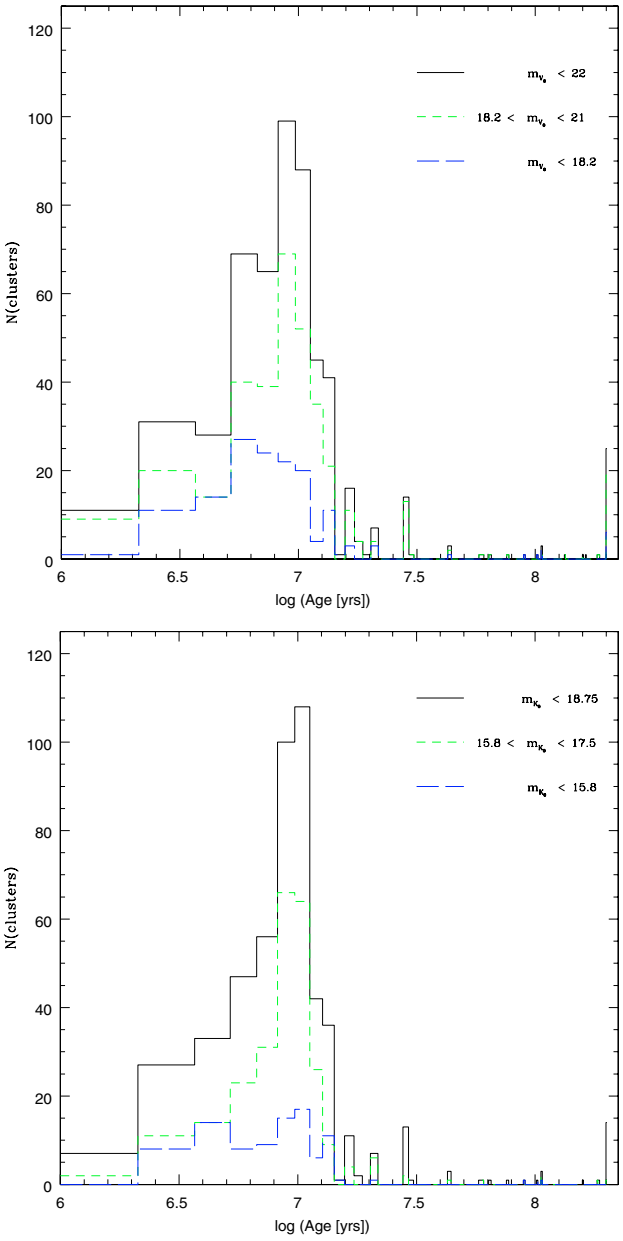

Fig. 9. Histogram of numbers of star clusters observed in each age bin. All clusters are young, and most clusters are either around 10 Myr or around 6 Myr old. Different colours/line-types differentiate between V-selected brightness limits (*top*) and Ks-selected (*bottom*). The strong peak of clusters of age 10 Myr is a selection effect introduced by detecting clusters in Ks-band, which has a strong peak in absolute luminosity around that age, caused by high-mass stars entering the red supergiant phase. This means that many low-mass clusters are detected in that age bin that would be below the detection limit at other ages (also see Fig. 10). Note the increasing relative number of young clusters (≈4 Myr) when going to brighter clusters in *both* figures, which is already an indication that more clusters are present at younger ages, even more convincing support for this being displayed in Fig. 11.

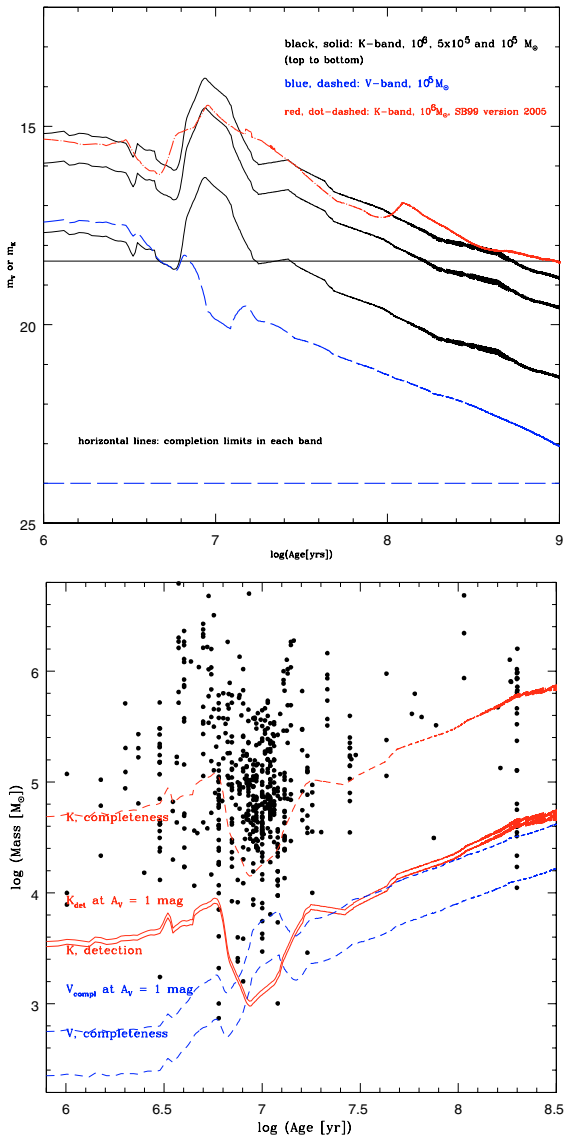

Fig. 10. Two different representations showing the completeness and/or detection limits for V and Ks band for our clusters. The upper graph shows completion limits for clusters with different total masses in V- and Ks-band. Both lower curves are for a 1×10^5 $M_\odot$ cluster, while for Ks-band, we added 5×10^5 $M_\odot$ and 1×10^6 $M_\odot$. This shows that in V-band, 50% of all clusters above a mass of 1×10^5 $M_\odot$ can be detected up to an age above 1 Gyr, whereas this cluster would drop below the Ks-band completion limit already at 25 Myr of age. The red (dot-dashed) line was, created using a Starburst99 (Leitherer et al. 1999) model, but this time for v5.0 (Vazquez & Leitherer 2005), which, amongst other modifications, includes the TP-AGB phase, which is responsible for the bump after 10^8 yr. The lower graph supports our claim that many more clusters exist with ages below 25 Myr, and that this is not a simple selection effect, because it shows that clusters above a certain mass (but for comparison needs to be above the completeness- or detection limit for all ages then) are much more numerous below 25 Myr than above that age. In Fig. 11, this claim becomes even more obvious.

broadband determined value by averaging the fluxes and converting back to magnitudes.

As could be expected from just looking at the false colour image (Fig. 12), extinction is very variable within the merger, peaking at extreme values of A_V above 10 mag in the overlap region. All extinction values quoted in this article assume a foreground screen extinction model.

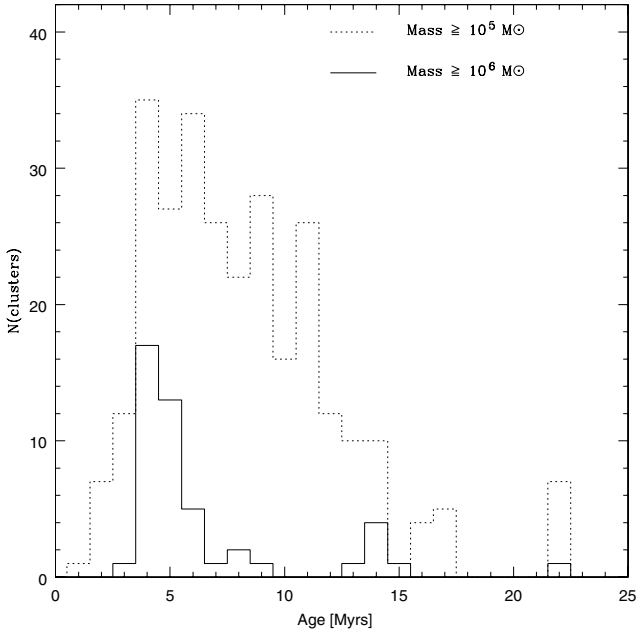

Fig. 11. Distribution of clusters above certain mass limits (10^5 and 10^6 $M_\odot$, respectively), as a function of age up to an age of 25 Myr, the age where a cluster of 10^5 $M_\odot$ reaches the *K*s-band completeness limit. This means that in our plot, essentially all clusters above the given mass limits should be detected, if they are present. The strong decline in cluster numbers up to an age of 15 Myr therefore means that indeed many more clusters are present around 6 Myr, meaning that either more clusters were produced or that a large fraction has been destroyed on timescales of 10−15 Myr.

The distribution of extinction is shown in Fig. 13, where we plotted a colour-coded map of A_V determined from the broad-band fit and, where possible, in combination with the line ratio value. Underlying this distribution is the false colour image from Fig. 12, to demonstrate the excellent agreement between high extinction clusters and dust lanes.

The average extinction is around $A_V = 1.3$ mag, and it is interesting to analyse the age dependence of the extinction distribution, reproduced in Fig. 14, for information about the clearing time of the clusters. The typical extinction decreases with increasing age, as can be seen in Fig. 14, which shows the median extinction values as a function of age in bins of 2 Myr, together with the individual data points which were used in the median. See Sect. 4 for an analysis of this evolution.

These age-averaged numbers artificially increase the extinction values for older clusters, at least if the purpose of the analysis is to determine the extinction directly related to the cluster in question, for example arising from its own dust cocoon. This is suggested by Fig. 15, where visual inspection of the locations of high- and low-extinction clusters above 9 Myr with respect to the locations of young, high-extinction clusters show that the high extinction older clusters appear almost exclusively in the direct vicinity of younger clusters. We took this as an indication that they only happen to lie within or behind the molecular cloud related to the formation of the younger, neighbouring cluster.

In an attempt to quantify the robustness of this visual impression, we calculated (via a two-dimensional K-S-test) the probability that the population of clusters that are young (age < 9 Myr) and highly extinguished ($A_V > 1.5$ mag), old (age > 9 Myr) and highly extinguished ($A_V > 2.0$ mag), or old with low extinction ($A_V < 0.8$ mag) are all spatially distinct. Our visual impression is confirmed. We find that the probability that the young and highly extinguished and the old and highly extinguished to be spatially distinct to be very low (only 22%). Thus it is likely that these clusters are drawn from the same sample. However this is not the case for the young and highly extinguished clusters and the old clusters with low extinction. These samples have a probability of $\ll$1% of being drawn spatially from the same population.

We plotted Fig. 15 with lower age limits for the "older" clusters increasing from 6 to 12 Myr in steps of 1 Myr (but we do not show these plots here), and the described effect becomes obvious between 8 and 9 Myr, which we interpret to be the time when most star clusters have cleared away their natal dust cocoon. This is the same age range suggested by Fig. 14.

Mostly caused by extinction, a fraction of the *K*s-band detected clusters is not detected at shorter wavelengths. To estimate the impact extinction has on cluster detection and on estimates of, for example, star formation rates based on observations in certain optical bands, we determined which fractions of clusters were undetected, how much mass they contribute, and how this compares to the mass which would be derived for the total cluster mass if only the observed light in clusters for the given band is used for mass determination.

Table 3 shows that the total fraction of clusters undetected in any given optical band, compared to the *K*s-band, is rather low, despite the sometimes fairly high extinction, thanks to the fact that the HST observations are up to a few magnitudes deeper. Even in *U*-band, only 16% of the clusters are not detected at all, and those clusters contribute only 12% of the total mass in clusters. These numbers become even more favourable going to *V* or *I* band.

The impact of extinction becomes obvious, however, if one compares the masses that would be derived from optical cluster light without applying an extinction correction. Using the individual cluster ages to derive individual cluster masses from just the observed magnitudes, like we did for *K*s-band, *U* and *B* bands lead to a total mass estimate that is just a quarter of the mass derived from *K*s, which improves only slightly towards *V* and *I* band, where a third of the *K*s-band mass is derived.

Not taking the individual age information into account, but instead assuming average ages and extinction can lead to more or less arbitrary results. For example, assuming an average age of 5 Myr for the clusters and converting the observed *U*-band flux to a total mass yields 33% of the mass derived from the extinction corrected *K*s-magnitudes (*K*s-mass), whereas assuming an average age of 25 Myr and an average extinction of A_V of 1 mag gives 9 times the *K*s-mass.

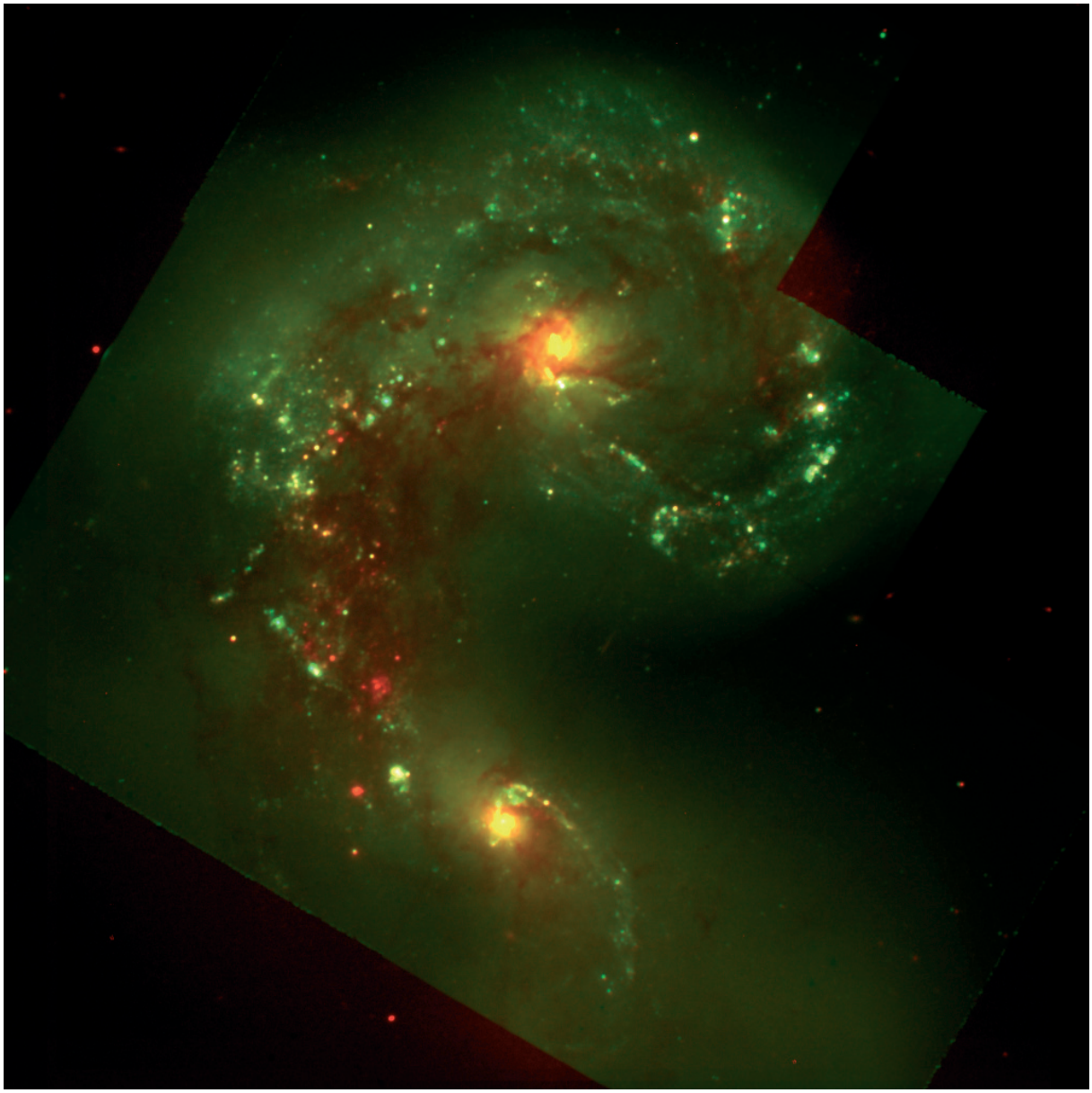

Fig. 12. False colour image of NGC 4038/39 with $U + B$ in the blue, $V + I$ in the green (these four images were obtained from the HST archive, see W99 for details) and Ks (ISAAC, VLT) in the red channel. Most of the reddening seen in the clusters in the "overlap region" between the two nuclei (and elsewhere in the merger) is caused by dust absorption and therefore gives a first-glance impression of the patchy and partially high extinction encountered in the merger, which was the main driver for obtaining our near-infrared observations. *FWHM* of the PSF is 0.″4 (HST images were smoothed), the region displayed covers approximately 2×2 arcmin, north is up, east to the left.

3.7. Photometric masses

Knowing the ages of the clusters is the presupposition for determining their photometric masses, $M_{\rm phot}$. The extinction corrected Ks-band magnitudes are compared to those expected for a cluster of a given age and mass for the model parameters. We use Ks-band magnitudes, rather than any of the optical colours for two reasons. First, in Ks-band all of our clusters are detected, so it is not necessary to extrapolate to one of the optical colours for an assumed age and extinction, which always introduces additional uncertainties. And second, Ks-band is much less affected by extinction, which additionally minimizes the uncertainties.

The Starburst99 (Leitherer et al. 1999) model parameters we used were again instantaneous burst, solar metallicity, and an IMF with Salpeter slope between 1 and 100 $M_\odot$; note that for an IMF extending between 0.1 and 100 $M_\odot$, the photometric masses would increase by a factor of 2.6. From the resulting individual cluster masses, we determine the total mass of stars produced in clusters during this starburst and the corresponding star formation rate (or rather, lower limits to both, since there are still many clusters expected to be below the detection limit), and a cluster mass function, which we compare to the luminosity function.

The total mass produced in Ks-band detected clusters with an age determination is $\approx 430 \times 10^6$ $M_\odot$. The error introduced

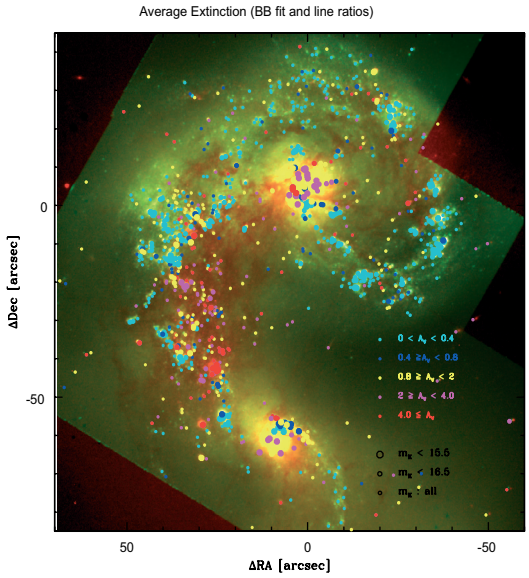

Fig. 13. Spatial distribution of extinction values (A_V) determined for the clusters. Values from the broadband fit and from the line ratios were combined to a common average where this was possible. Note the excellent agreement between high extinction values (red and magenta dots) and the lanes of dust obvious in the multi-colour image (the same as in Fig. 12, only with different cut levels).

by not taking those clusters without age determination into account is fairly small, since it is mostly the faint, low mass clusters which lack an age estimate. And, as mentioned above, the SFR we determine here will be a lower limit. From Fig. 9, we see that the bulk of star clusters are younger than 25 Myr, which yields an SFR of $SFR_{\rm clusters} \approx 16\ M_\odot\,{\rm yr}^{-1}$, which is almost 20 times the Milky Way SFR, and a moderate to normal value for a starbursting galaxy. Interestingly, the total molecular gas mass estimated for the Antennae is approximately $10^{10}\ M_\odot$ from CO observations (Wilson et al. 2001), which is substantially greater than the estimated total cluster mass – approximately a factor of 10−20 of the cluster mass reported here (depending on whether the IMF is Salpeter from 1−100 $M_\odot$ or a reasonable extrapolation like a Kroupa IMF with a minimum mass of 0.1 $M_\odot$).

Thus the current gas depletion time would be about 250 to 500 Myr, if a star formation efficiency of 100% was assumed. For a more reasonable assumption on the star formation efficiency, like 30%, the depletion time needs to be scaled down accordingly, but in any case, this further supports intense star-formation over the expected merger time scale.

Taking our conclusions into account concerning cluster dissolution, and instead assuming constant star formation over the last 25 Myr, our lower limit concerning the star formation rate increases by at least a factor 2.5, and would then be above 40 $M_\odot\,{\rm yr}^{-1}$.

3.8. Cluster mass function

The cluster mass function in merging galaxies is of special importance with respect to star cluster formation and evolution, because globular cluster mass functions and their luminosity functions (with a small age range) are Gaussian (or similarly single-peaked), with a typical mass around $2 \times 10^5\ M_\odot$. However, luminosity functions of clusters in merging galaxies show a power law with a typical slope $\alpha = -2$. Cluster mass functions are difficult to determine, as in this work, because it requires the determination of individual ages for these young clusters where the intrinsic luminosity varies strongly with age. Nevertheless, the mass function for the Antennae clusters was constructed from HST data by Zhang & Fall (Zhang & Fall 1999), and found to be a power law with approximately $\alpha = -2$ with no indication of a turnover at any mass. A turnover of power laws is consistent with the luminosity function constructed from the same data by Whitmore et al. (1999) with the turnover roughly at $1 \times 10^5\ M_\odot$, comparable to the characteristic mass of globular clusters mentioned above.

From our *K*s-band data, we created the luminosity- and mass functions, and even though the data are shallower in limiting magnitude, we hope to benefit from the decreased influence of extinction on our data. Luminosity and mass functions are displayed in Figs. 16 and 17. The assumption that a large fraction of the highest mass clusters could be composed of cluster complexes, rather than individual clusters, could be excluded by visual inspection of both, the *K*-band image and the higher resolution *I*-band image at the locations of the high-mass clusters. At least down to the spatial scales which can be resolved, less than 5% of the clusters with masses above $10^5\ M_\odot$ look like they might be affected by multiplicity. However, very close binary clusters (like for example NGC 1569A, which could be resolved into two components with a separation of 0.″2 on HST images (see de Marchi et al. 1997)) cannot be excluded for the Antennae clusters, which lie at almost 10 times the distance of NGC 1569.

The extinction corrected *K*s-band luminosity function of star clusters in NGC 4038/4039 can be fit by two power laws ("broken power law") with a turnover magnitude of $m_{Ks} = 15.45$, and the slopes $\alpha = -2.6$ and $\alpha = -1.37$, respectively. The slopes compare fairly well with those determined by Whitmore et al. (1999) from the objects located on the PC chip, which had been confirmed to be star clusters from an analysis of their *Q*-parameters. This fact is somewhat surprising, because the turnover masses in the *K*s- and *V*-luminosity functions need not necessarily be the same, since the cluster luminosity function is a function of cluster ages (therefore mass-to-light-ratios) and masses.

Comparing the absolute turnover *K*s magnitude of $M_{Ks} = -15.96$ mag to that of a $10^6\ M_\odot$ cluster of the median age of 9.2 Myr ($M_{Ks} = -17.52$ mag) yields a turnover mass of $2.4 \times 10^5\ M_\odot$. This could be interpreted as the progenitor to the typical mass peak in the globular cluster mass function.

In Fig. 17, the cluster mass function can also be fit by a broken power law, with the two slopes of $\alpha = -1.9$ and $\alpha = -1.2$. The turnover mass here is around $3 \times 10^5\ M_\odot$, which is in reasonable agreement with the value derived from the luminosity function. However, as we will discuss in Sect. 4, we do not want to overinterpret this result, since both random and systematic uncertainties are rather large, and the latter difficult to overcome.

Table 3. Comparison of the photometry of detected and undetected clusters in the optical bands to the *K*s band. The first column gives the names of the bands (rather, the Johnson equivalents to the HST broadband filters), the second column gives the number of *K*s-detected clusters which are not detected in the specified band (in percent). The *K*s-mass referred to in Cols. 3 and 4 was obtained in the following way: the extinction corrected *K*s-magnitudes for individual clusters were compared to the magnitude expected for a cluster of 1×10^6 $M_\odot$ (using Starburst99 for an instantaneous burst, solar metallicity, Salpeter IMF between 1 and 100 $M_\odot$). These masses were summed up to derive the total *K*s-band mass. Column 3 is the total *K*s mass of the clusters not detected in the specified band, whereas Col. 4 specifies the mass of all the clusters detected in the given band, if only the not extinction corrected flux in the given band is used (together with cluster age) to determine the mass.

Band	number of clusters detected in *K*s, but not in Band	mass of clusters not detected in Band over *K*s mass	mass derived from $m_{\rm Band}$ and age over *K*s-mass
U	16%	12%	26%
B	13%	10%	27%
V	6%	5%	33%
I	9%	6%	33%

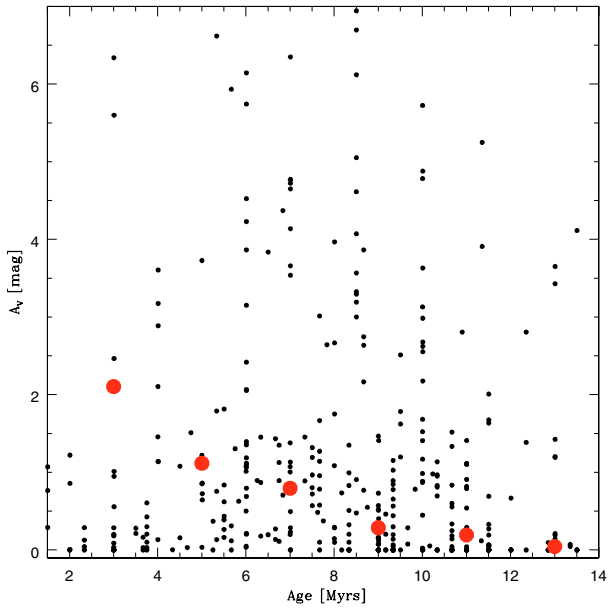

Fig. 14. Small black dots: individual $A_{\rm V}$, age data points for clusters with good age estimates. Large red dots are the medians of extinction values found in 2 Myr wide bins, where the last bin shown contains 36 data points, many of which have $A_{\rm V}$ close to 0 and therefore overlap. Despite the large scatter in $A_{\rm V}$ values in any given age bin, the expected trend of lower $A_{\rm V}$ with increasing age is obvious, and many of the clusters older than 8–9 Myr have very low extinction. This further supports the idea that this is the age where many of the clusters emerge from their natal dust cocoon.

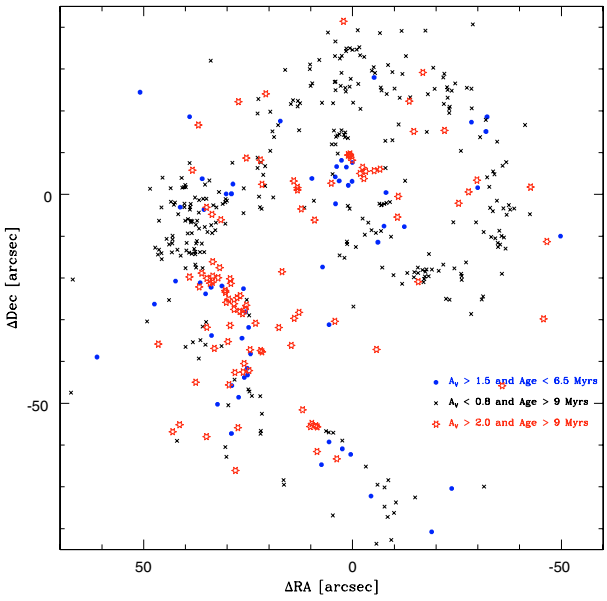

Fig. 15. Extinction values colour coded in their distribution in the Antennae. The 10 Myr clusters with high extinction are preferentially located near younger clusters, while those with low extinction values are often either single or in groups of older clusters.

3.9. Bolometric luminosity

We used the combination of individual photometric masses and ages to determine the bolometric luminosity expected to be emitted from a given cluster, using the predictions from Starburst99 (Leitherer et al. 1999), where the bolometric luminosity is obtained by integrating the spectral energy distribution without the nebular continuum. From this, we created an artificial "bolometric image" to compare it to the ISOCAM 15 μm image (Mirabel et al. 1998, see also the comparison of 15 μm image and CO map in Wilson et al. 2001), to the radio continuum emission observed by Neff & Ulvestad (2000) and to CO emission (Wilson et al. 2001).

Our main goal here was to see whether the mass and age of the very red star cluster eastward of the southern nucleus (WS95-80) justifies its being the brightest object in the merger at 15 μm and how in general the 15 μm emission relates to the expected bolometric flux. What we found is that WS95-80 is indeed expected to be a bolometrically bright object, amongst the brightest sources in the Antennae, but not as bright as expected from the 15 μm image. While we would expect it to contribute 3.6% to the total flux at 15 μm, Mirabel et al. (1998) measured it to contribute roughly 15%. Measurements concerning the contribution of the overlap region as a whole are more in agreement; while they measure ≈50%, we would expect 43% of the bolometric luminosity to originate in that ≈3 kpc × 5 kpc large region.

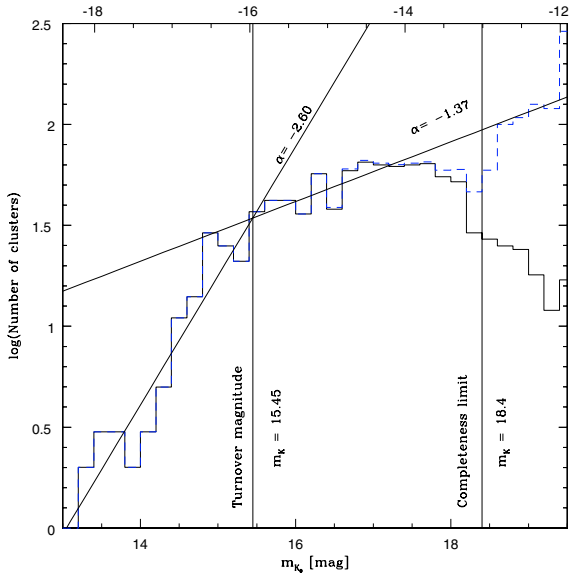

Fig. 16. Extinction corrected Ks-band luminosity function of star clusters in NGC 4038/4039. Completeness limit (50% of clusters detected) and completeness corrected data points are indicated. The data can be fit by two power laws with a turnover magnitude of $m_{Ks} = 15.45$. Comparing the corresponding absolute Ks magnitude of $M_{Ks} = -15.96$ mag to that of a 10^6 $M_\odot$ cluster of the median age of 9.2 Myr ($M_{Ks} = -17.52$ mag) yields a turnover mass of 2.4×10^5 $M_\odot$.

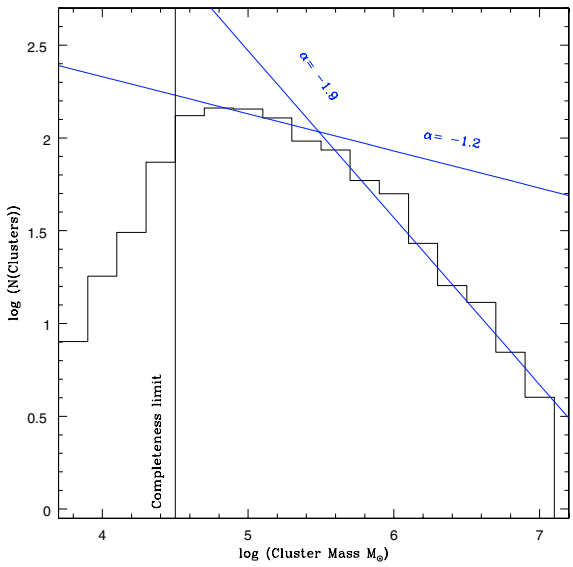

Fig. 17. Mass function of Ks-band detected star clusters in NGC 4038/4039, and fits using two power laws (slope −1.9 and −1.2). Masses were determined using individual cluster ages and comparing the observed magnitudes to those predicted by Starburst99 for a 10^6 $M_\odot$ cluster. The completeness limit is not exact, because it is the completeness limit in magnitudes (see Fig. 16) which was converted to a mass for the median cluster age of 9.2 Myr. For some ages which are quite well represented, for example around 6 Myr, the completeness limit lies rather around 10^5 $M_\odot$, which makes it really difficult to apply a completeness correction for this plot, which we therefore omitted. Also these data can be fit by two power laws, with a turnover mass around 3×10^5 $M_\odot$, in reasonable agreement with the number derived from the luminosity function.

4. Discussion

4.1. Age distribution of the young clusters

As shown in Sect. 3.5, based on Figs. 9–11, about 70% of the K_s-band-detected star clusters with masses $\geq 10^5$ $M_\odot$ are younger than 10 Myr. Thus, 10 Myr is approximately an e-folding time for ages of the most massive clusters. Unfortunately, our information about lower mass clusters is severely biased by the form and sensitivity of mass-to-light ratio in the K-band with age.

There are two plausible hypotheses for explaining this rather narrow range of ages of the Antennae clusters: either at least 70% of the clusters have been produced within the last 10 Myr, or the e-folding survival time for the ensemble of clusters is about 10 Myr. A short survival time would mean that either the clusters are born unbound or some process efficiently destroys what are otherwise bound clusters at birth. We note again that we can only make this statement firmly for clusters above $\approx 10^5$ $M_\odot$, which lie above the Ks-completeness limit out to ages of around 25 Myr. But even considering incompleteness, the number density of older clusters below our completeness limit still decline and thus it is probably safe to extend the age limit for determining the number of clusters out to an age of ≈100 Myr.

4.1.1. Cluster age distribution as star-formation history

The changing gravitational potential in a strong merger like the Antennae can induce strong variations in the star-formation rate (e.g., Mihos et al. 1993). According to the most common models, closest passage of the two galaxies comprising the Antennae happened roughly 200 Myr ago (see e.g., Barnes 1988). At first passage pericenter, galaxy merger models predict strong star-formation which declines, and depending on the exact geometry and gas distribution, weaker peaks in the star-formation can occur (e.g., Mihos et al. 1993; Barnes 2004). This enhanced star-formation tends to persist for a factor of 0.5 to 1 dynamical times (the orbital time-scale of the first encounter, thus around 200−300 Myr) after the first passage pericenter. However, none of the models appear to show intense star-bursts that return to the star-formation rates before the strong interaction occurred. The contrast between peaks in the star-formation and the low points during the merger range about a factor of a few and always well above the rate before the strong interaction occurred. In addition, none of the peaks modelled appear to last less than 5% of dynamical time.

The e-folding timescale of 10 Myr, which we estimate for the clusters currently observed in the Antennae, is short compared to the dynamical time of the Antennae. In the model of Mihos et al. (1993), the periapse of the Antennae occurred about 200 Myr ago and the galaxies will merge in about 100 Myr. Thus the e-folding time of the cluster ages represents something less than 5% of the dynamical time of the merger. This is short. The disks of NGC 4039/39 should have hardly felt a change in the potential. Nevertheless, clusters with identical ages are distributed throughout the face of the system,

which is hard to explain as a "coordinated" burst, because the communication time between the regions is longer than the age spread.

It is possible that the interaction has produced other sources of perturbations like spiral density waves in the disks or bars. These could also act to induce star-formation. But once again, the dynamical time scale for spiral density waves is similar to the dynamical time of the disks themselves, which are on the order of 100 Myr or longer. Bars can have shorter time scales (10 s of Myr), but would lead to star-formation which is largely circum-nuclear. One of the striking aspects of the star-formation in the Antennae is that it occurs throughout the disks. Moreover, we do not observe a large range of ages across the face of the Antennae, as might be expected by gravitational perturbations. Since the timescales are long, we would expect the age range to be a significant fraction of these timescales. While we do observe that the clusters are younger in the "overlap" region, this is only at the level of a few Myr. Given the disparities in the various dynamical timescales, the relatively short e-folding time of the cluster ages, and the narrow range of ages across the Antennae, it appears unlikely that the narrow range of ages reflects the star-formation history within the Antennae.

4.1.2. Cluster age distribution as cluster destruction time-scale

On the other hand, there are mechanisms which could lead to the destruction of clusters on a variety of time scales. The possible mechanisms include, roughly in order of increasing time scale: clusters being born un- or marginally bound, rapid loss of natal material, mass loss through stellar evolution, stellar ejection during 2-body relaxation, clusters being born with a significant fraction of their binding energy in "hard" binaries, tidal interaction with nearby clusters or gravitational perturbations such as bars or spiral arms, and gravitational shocks. Of course, rapid destruction as constrained by the clusters in the Antennae may require several of these to act in unison.

The simplest hypothesis to explain the short timescale during which the clusters must be disrupted would be that they are not gravitationally bound when they form. If true, this would present a very interesting quandary given that they are very dense stellar systems. A model for star-formation has been proposed where the driving force is supersonic turbulent convergence flows in the interstellar medium (see the excellent review by Mac Low & Klessen 2004, and references therein). A situation like that, as opposed to gravitational collapse with fragmentation, may lead to compact, vigorous star-formation as observed in the young compact clusters in the Antennae, but with the stars that formed not bound as a single entity.

In Mengel et al. (2002) we estimated that the crossing time for massive clusters in the Antennae of $\tau_{CR} = R_{1/2}/\sigma \approx$ few$\times 10^5$ yr. The crossing for less massive clusters than studied in Mengel et al. (2002) will be roughly similar, since they have roughly similar mean densities. Following Fall (2004), if a cluster is approximately freely expanding as a result of catastrophic mass loss or of being born unbound, the characteristic radius increases as $R_{1/2}(t) \approx R_{1/2}(0)(\tau/\tau_{CR})$, and its characteristic surface density decreases as $\Sigma(t) \approx \Sigma(0)(\tau/\tau_{CR})^{-2}$. Thus after 10−100 cross times, the characteristic radius has increased by that amount, and the characteristic surface density would be a factor of 100 to 10 000 lower (5−20 mag). The size of these effects means that clusters would drop below our detection limit in only a few crossing times.

The magnitude of this effect means that it can be tested observationally. In Mengel et al. (2002) we used an analysis of the compactness, velocity dispersion, and IMF of some of the most massive young ($\lesssim$10 Myr) clusters in the Antennae to argue that the clusters must be relatively long lived (survival more than several 100 Myr). This conclusion was reached under the assumption that the clusters are initially bound and then subsequent stellar evolutionary and dynamical processes are the only effects that lead to the dissolution of the clusters. This study was also limited to a small number of clusters and certainly could have been biased to those that are long lived; the ages of the clusters studied were all close to 10 Myr. The results presented here allow us to address this question with greater statistical power. If the cluster were unbound or dissolving due to internal mass loss (stellar evolutionary and dynamical), we would expect the cluster to expand and its concentration to go down with age. As argued previously, if the clusters were initially unbound and freely expanding the concentration would decrease rapidly with time. In an attempt to determine whether the cluster size or concentration changes with age, which might indicate of cluster disruption if older clusters are generally more expanded or shallower than younger clusters, we measured cluster sizes and King concentration parameters for clusters in two of our age bins for the K-detected clusters: younger than 4 Myr (7 members measured) and between 8 and 11 Myr (11 members measured). In principle, we would have liked more and narrower age bins in order to check for an evolution of size with age, but there are not enough I-band bright, isolated clusters to fill these bins in statistically relevant numbers, therefore we used these two clearly separate age bins.

Our result was that the spread in cluster sizes and concentrations is large for both groups (in the results, we quote the standard deviation), but that the average sizes are smaller for the older group, and they tend to be more concentrated. Young clusters have $R_{\rm eff}$ = 16 pc (±15 pc), King concentrations 15−40, while older clusters have $R_{\rm eff}$ = 6.5 pc (±5.3 pc), King concentrations 7−27. If the clusters were simply freely expanding, the effect should be strong and obvious. Thus free expansion seems unlikely. These results do not lead to a clear interpretation for other processes that might lead to rapid dissolution and whose effects are less obvious. Either cluster evolution generally concentrates the clusters or the weakly concentrated clusters get disrupted, which decreases the size average for the survivors.

For clusters which are not very concentrated after formation and/or had a shallow IMF, relaxation processes can lead to destruction on timescales of a few tens of Myr (see, e.g., Takahashi & Portegies Zwart 2000; Mengel et al. 2002). Relaxation processes could lead to rapid cluster destruction if the cluster is only marginally bound, as might be the case, say, for a strong convergence flow like formation mechanism

Mac Low & Klessen (2004). Given there is no clear dependence with age on any of the parameters measured, we have no unambiguous answer to what process is dominant. Processes that lead to rapid dissolution short of free expansion are (i) stellar mass loss (winds and supernova) that both reduce the stellar mass and remove the natal material (in conjunction with the radiation pressure) and (ii) relaxation processes (e.g., 2-body relaxation, interactions with hard binaries) that preferentially eject the low mass stars. Dissolution of clusters is enhanced for clusters with shallow IMFs and low stellar concentrations (Vesperini & Zepf 2003). So a plausible explanation for the generally rapid dissolution of a significant fraction of the clusters is that some are marginally bound, and thus the processes such as loss of the natal material, stellar evolutionary-driven mass loss, and dynamical mass loss all become more effective and more efficient in unbinding some of the clusters.

If rapid dissolution of young compact clusters[3] – which is also a favoured scenario for Fall and Whitmore (see Fall 2004; Whitmore 2004, which also focus on the clusters in the Antennae) and for Bastian et al. (Bastian et al. 2005, which analyzes the cluster population in M 51) – is common to all merging galaxies, then estimates of the fraction of star-formation in mergers (and perhaps other types of star-bursts) that occur in such clusters are likely to be severely underestimated. For example, Meurer et al. (1995) estimated that about 20% of the UV light from starbursts comes from young compact star clusters. This would suggest that either there is background star-formation that does not reach the high stellar densities of the young compact star-clusters or that the background light is composed of stars from dissolved clusters. Our results indicate that this is most likely the case. Indeed, Tremonti et al. (2001), in a UV spectroscopic study of cluster and background populations in the dwarf galaxy NGC 5253, found a relative paucity of O-stars in the background population compared to the compact clusters. They interpreted this difference as background light (non-cluster light) due to clusters that dissolved on the order of 10 Myr. Combined with our direct statistical evidence for cluster destruction (see also Zhang & Fall 1999; Fall 2004), this provides powerful evidence that both lifetime of clusters is short and that cluster formation must be a very significant mode of star-formation in all star-burst galaxies.

4.2. Nature of brightest 15 μm peak

With its observed age of 4 Myr and a photometric mass of just above $7 \times 10^6\ M_\odot$, cluster WS95-80 is expected to have a bolometric observed magnitude of $m_{\rm bol} = 11.4$ mag. This is far less than what is expected from the 15 μm image, where it contributes 15% of the total flux from the merger (Mirabel et al. 1998). This discrepancy supports a suggestion made by Wilson et al. (2001) for the origin of the strong 15 μm emission. One of their two options was that the giant molecular clouds, three of which seem to be overlapping or colliding in this location, efficiently transport very small dust grains into the vicinity of the hot stars that are present in the relatively young (4 Myr) star cluster. There, they are heated up to ≈100 K, which leads to strong continuum emission around 15 μm (the spectrum is observed to be rather steeply rising in that region). For their other option, that of an even younger star cluster (younger than 1 Myr), we see no evidence, even in *K*s-band or, from visual inspection, in the 8 μm Spitzer image presented by Wang et al. (2004).

We identify two other regions where we might expect a strongly rising continuum in the 15 μm range: roughly in the middle of the overlap region and to the southwest of the northern nucleus (marked with arrows in Fig. 18). Both of these locations, like cluster WS95-80, have a 15 μm flux which is substantially brighter than the one expected from the artificial bolometric image. We did not analyze the ISO data for these regions, but it could be worthwhile checking whether they show the same spectral signature as No. WS95-80. It may be significant in that context that all three regions which we marked in Fig. 18 are star clusters that lie just on the edge of a rather steep increase in CO flux.

Concerning the coincidence and offset between CO intensity and simulated $m_{\rm bol}$ (see Fig. 20), we see this in the context of the age distribution in the Antennae. The overlap region, which hosts the youngest clusters, shows a clear correlation between CO flux and the location of the clusters (as traced by the bolometric luminosity), which is not the case for the northwestern region. There, most of the clusters are instead around 10 Myr old, an age where they have blown free of their natal dust clouds, which can explain the observed offset.

4.3. Extinction evolution

In Sect. 3.6 we gave two pieces of evidence that clusters are usually formed in high extinction regions and have cleared away this natal dust cocoon by the age of 8–9 Myr. First evidence is the correlation between high-extinction older clusters with high-extinction young star clusters. This we interpret to mean that a cluster of around 10 Myr or older which suffers high extinction is often no longer obscured by its own dust cocoon, but just happens to be located in a region of more recent star formation, where the dust content is still generally high. This effect is not seen for clusters below 8 Myr and sets in around 9 Myr, therefore the clusters on average seem to clear away their natal cloud around that age.

The same result is obtained from Fig. 14, where – despite large variations in $A_{\rm V}$ within each age bin – the evolution of extinction with age clearly declines. Also here, 8–9 Myr is approximately the limiting age above which many clusters have a sufficiently low extinction to be certain that they have emerged from their natal dust cocoon.

4.4. Impact of extinction

As shown in the previous section, owing to extinction a careful analysis of the optical data is required if sensible parameters, such as total masses and thereby star formation rates, are to

[3] The first reference we are aware of mentioning a dissolution timescale of ≈10 Myr was made by Lada & Lada (2003) for Galactic open clusters and therefore not strictly relevant to our compact, massive targets.

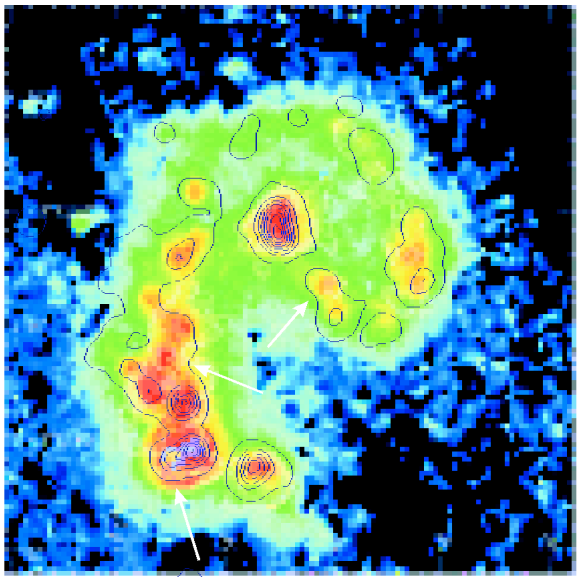

Fig. 18. Overlay of ISOCAM 15 μm image (Mirabel et al. 1998) with simulated $m_{\rm bol}$ contours, created by calculating the expected bolometric magnitude of each *K*s-detected cluster and feeding this, together with the position, into the IRAF *daophot.addstar* routine. The resulting image was then Gaussian smoothed to have a resolution comparable to the ISOCAM 15 μm image. Arrows indicate the three regions: bottom arrow shows the brightest 15 μm cluster, which does *not* have the highest bolometric luminosity, while the other two indicate other regions where the simulated bolometric luminosity is substantially lower than expected from the 15 μm flux.

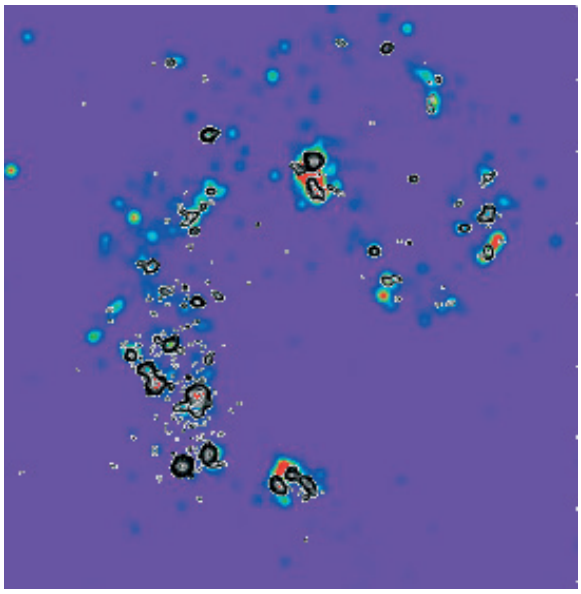

Fig. 19. Overlay of our simulated $m_{\rm bol}$ image, slightly less smoothed than in Fig. 20, with radio 6 cm contours (high-pass filtered, so it shows predominantly the point-like sources) (from Neff & Ulvestad 2000, their Fig. 4c). The radio continuum emission here consists mostly of free-free emission of gas photo-ionized by hot stars, therefore it is considered a good tracer of recent star formation. Note the excellent correspondence between the two maps.

be derived from optical wavelengths alone in galaxies like the Antennae.

Here, a combination of considerably deeper optical images and a moderate ($A_{\rm V} \approx 1.3$) average extinction means that only a small fraction of clusters which are detected in *K*s is undetected in the other bands. This holds even for *U* band (see Table 3). However, converting the observed cluster magnitudes into a quantity like mass without information on the extinction leads to unacceptable uncertainties. This is even the case if age information of the single clusters is taken into account. In that case, the mass, assuming zero extinction, will always be underestimated. In our case, only a quarter of the mass is derived from *U* and *B* observations.

Even worse results are obtained if average ages and extinctions are assumed; then for more or less reasonable assumptions for these averages, the derived total mass can easily vary by orders of magnitude. This behaviour will be less extreme in galaxies where the major star formation event is not equally young, because after a few hundred Myr, the luminosity evolution of a star cluster is much slower.

On the bright side, we showed in the previous section that it is possible to obtain reasonable estimates of both, ages and extinction, of these simple stellar populations by fitting the observed broadband colours with these two free parameters. However, it is crucial there to have a broad wavelength baseline; therefore optimally one needs a detection in both *U* and *K* bands, or at least in one of them.

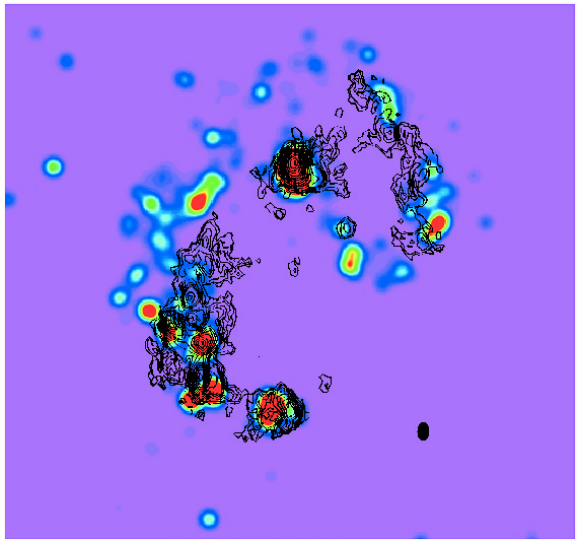

Fig. 20. Overlay of our simulated $m_{\rm bol}$ image with CO contours from Wilson et al. (2001) to compare with Fig. 18, where the $m_{\rm bol}$ image is slightly more smoothed. Note the good agreement in the overlap region, whereas the north-western region shows a significant offset between the clusters and the CO peaks. The three regions with arrows in Fig. 18 all lie in regions where a star cluster lies just on the edge of a relatively sharp edge in the CO map. The black ellipse shows the beam size of the CO observations.

4.5. Luminosity- and mass function

As shown in Sect. 3.7, we constructed luminosity- and mass functions for our *K*s-detected clusters. Even though both functions can in principle be fit by broken power laws with turnover cluster masses of 2.4 and 3×10^5 $M_\odot$, respectively, we caution

that both functions do not allow for this straightforward interpretation.

While the luminosity function is easily constructed and also completeness correction is relatively easy, it is not very meaningful to compare this luminosity function to, for example, that of globular cluster systems, because the strong variation of mass-to-light ratios between the clusters building up this luminosity function means that a given luminosity cannot reliably be converted into a cluster mass. The observed "turnover mass", where the two power laws that were fit to the function cross, is converted into a characteristic mass assuming the mass-to-light ratio of the median cluster age in our sample (9.2 Myr) but particularly the high luminosity clusters are often rather around 6 Myr old, where the mass-to-light ration differs from that at 9.2 Myr substantially.

The mass function has a similar problem. While it is simple to construct a mass function from those clusters, which had ages and extinctions assigned and therefore an individual mass estimate, it is difficult to apply a completeness correction. Even though above $\approx 10^5\ M_\odot$, the mass function should be complete for all ages, the completeness limit for the median age lies around $3\times10^4\ M_\odot$, but in the mass range between these two values, the mass function will be affected by those clusters which have ages where the completeness limit lies in that mass range. And from the mass function strictly above $10^5\ M_\odot$, one cannot reliably determine a turnover, expected to lie between 1 and a few times $10^5\ M_\odot$. Data that do not accurately probe the turnover provide very little constraint on the overall mass function.

As a result, even though we constructed the luminosity- and mass functions, mainly for the sake of comparison with what other authors found (Whitmore et al. 1999; Zhang & Fall 1999, for the luminosity and mass function, respectively), and also find good agreement at least for the luminosity function, we caution not to take these results too seriously. To improve the results, *K*-band observations would be required which go ≈2.5 mag deeper, pushing the completeness limit down to around $10^4\ M_\odot$ for all ages. And we note that without the near-infrared data, accurately accounting for the extinction is challenging, making it difficult to estimate robust total stellar masses for individual clusters.

Even though the required depth is provided by the optical HST data alone (Zhang & Fall 1999), we think that the broader wavelength coverage obtained by including the *K*-band substantially improves the age – and extinction –, and thereby the photometric mass determinations.

5. Summary

To summarise, our main conclusion from the analysis of VLT/NTT Antennae near-infrared images, in combination with the HST optical images, is that there is evidence that the majority of the bright, young cluster population will not evolve into globular clusters, but rather disrupt on timescales as short as tens of Myr. If this was a generic property of starbursts, the amount of star formation in similar events seems to have been underestimated so far.

Large uncertainties are also introduced into estimates of star formation rates if individual cluster ages and extinction are not taken into account. In detail:

- Most *K*s-band detected star clusters are young, with the median age ≈9 Myr and with a fairly narrow age range. Most of the youngest clusters (those below ≈5 Myr) are found in the so-called overlap region between the two galaxies. All other ages, also the few older clusters (up to 200 Myr) are relatively evenly distributed over the two galaxies. The numbers of young clusters peak at two ages, 6 and 10 Myr, the latter being mostly a selection effect (the clusters were detected in *K*-band).
- The most likely explanation for the narrow range of ages is that clusters are destroyed or dissolve on scales of a few 10 Myr. Analysis of the cluster concentrations as a function of age does not reveal a trend. Thus it is unlikely that the clusters are born freely expanding. More likely is that they are marginally bound and that stellar evolutionary and dynamical mass loss lead to clusters becoming quickly unbound. Thus whether a cluster dissolves is likely to be dependent on its mass distribution (concentration, etc.) and initial mass function.
- The extinction is variable, between $A_V \approx 0$ and more than 10 mag foreground screen extinction. The average value is 1.3 mag. It drops with increasing cluster age, which is consistent with the picture that a star cluster forms in a very dense and dust-enshrouded environment and blows free of this cocoon after a few Myr. Most clusters have reached this stage between the age of 8 and 9 Myr.
- Comparing photometry in the different bands, we note that information about age and extinction for individual clusters is necessary if meaningful conclusions about properties like total stellar mass in clusters or (clustered) star formation rate are to be obtained. Not taking this information into account, or assumption of average values can lead to results differing by orders of magnitudes. However, both age and extinction information can be obtained from broadband colours alone if the wavelength coverage is broad enough.
- A lower limit to the star formation rate over the last 25 Myr is $\approx 20\ M_\odot\ \mathrm{yr}^{-1}$, a relatively typical value compared to those for other nearby starbursts. But this is taking only the detected clusters into account and not correcting for any potential dissolution of clusters – including the latter, the lower limit for the SFR increases to $\approx 50\ M_\odot\ \mathrm{yr}^{-1}$.
- Even though the *K*s-band luminosity- and mass functions are best fit by broken power laws, and the turnover masses at face value lie around (up to factor of 2) the characteristic mass of globular cluster mass functions, this result should not be over-interpreted, due to limitations implied by systematic uncertainties.

Acknowledgements. Part of S.M.'s work was done at Leiden Observatory, The Netherlands, financed by the EU RT Network "Probing the Origin of the Extragalactic Background Radiation" and as a component of her Ph.D. Thesis work at MPE. We thank the ESO OPC for their generous allocation of observing time and the staff of Paranal and La Silla for their support during the observations

presented here. Finally, we would like to thank the referee, Peter Anders, for his insightful comments.

References

Anders, P., & Fritze-v. Alvensleben, U. 2003, A&A, 401, 1063
Anders, P., Bissantz, N., Fritze-v. Alvensleben, U., & de Grijs, R. 2004, MNRAS, 347, 196
Barnes, J. E. 1988, ApJ, 331, 699
Barnes, J. E. 2004, MNRAS, 350, 798
Barnes, J. E., & Hernquist, L. E. 1991, ApJ, 370, L65
Bastian, N., Gieles, M., Lamers, H. J. G. L. M., Scheepmaker, R. A., & de Grijs, R. 2005, A&A, 431, 905
Boily, C. M., & Koupa, P. 2003, MNRAS, 338, 665
de Marchi, G., Clampin, M., Greggio, L., et al. 1997, ApJ, 479, L27
Doyon, R., Joseph, R. D., & Wright, G. S. 1994, ApJ, 421, 101
Fabbiano, G., Zezas, A., & Murray, S. S. 2001, ApJ, 554, 1035
Fall, S. M. 2004 [arXiv:astro-ph/0405064]
Fall, S. M., & Zhang, Q. 2001, ApJ, 561, 751
Förster-Schreiber, N. M., Genzel, R., Lutz, D., & Sternberg, A. 2003, ApJ, 599, 193
Kleinmann, S. G., & Hall, D. N. B. 1986, ApJS, 62, 501
Kravstov, A. V., & Gnedin, O. Y. 2005, ApJ, 623, 650
Kroupa, P. 2001, MNRAS, 322, 231
Kunze, D., Rigopoulou, D., Lutz, D., et al. 1996, A&A, 315, 101
Lada, C. J., & Lada, E. A. 2003, ARA&A, 41, 57
Lançon, A., & Wood, P. R. 2000, A&AS, 146, 217
Landolt, A. 1983, AJ, 88, 439
Leitherer, C., Schaerer, D., Goldader, J. D., et al. 1999, ApJS, 123, 3
Mac Low, M.-M., & Klessen, R. S. 2004, Rev. Mod. Phys., 76, 126
Mathis, J. S., Rumpl, W., & Nordsieck, K. H. 1977, ApJ, 217, 425
Mengel, S., Lehnert, M. D., Thatte, N., Tacconi-Garman, L. E., & Genzel, R. 2001, ApJ, 550, 280
Mengel, S., Lehnert, M. D., Thatte, N., & Genzel, R. 2002, A&A, 383, 137
Meurer, G. R., Heckman, T. M., Leitherer, C., et al. 1995, AJ, 110, 2665
Mihos, J. C., Bothun, G. D., & Richstone, D. O. 1993, ApJ, 418, 82
Mirabel, L. F., Vigroux, L., Charmandaris, V., et al. 1998, A&A, 333, L1
Moffett, T. J., & Barnes, T. G. III 1979, AJ, 84, 627
Neff, S. G., & Ulvestad, J. S. 2000, AJ, 120, 670
Osterbrock, D. E. 1974, Astrophysics of Gaseous Nebulae (W. H. Freeman and Company)
Origlia, L., & Oliva, E. 2000, A&A, 357, 61
Origlia, L., Goldader, J. D., Leitherer, C., Schaerer, D., & Oliva, E. 1998, ApJ, 514, 96
Schulz, J., Fritze-v. Alvensleben, U., Möller, C. S., & Fricke, K. J. 2002, A&A, 392, 1
Takahashi, K., & Portegies Zwart, S. F. 2000, ApJ, 535, 759
Tremonti, C. A., Calzetti, D., Leitherer, C., & Heckman, T. M. 2001, ApJ, 555, 322
Vazquez, G. A., & Leitherer, C. 2005, ApJS, in press
Vesperini, E., & Zepf, S. E. 2003, ApJL, 587, 97
Wang, Z., Fazio, G. G., Ashby, M. L. N., et al. 2004, ApJS, 154, 193
Whitmore, B., & Schweizer, F. 1995, AJ, 109, 960
Whitmore, B. C. 2004, in The Formation and Evolution of Massive Young Star Clusters, ed. H. J. L .L. M. Lamers, L. J. Smith, & A. Nota (San Francisco: Astronomical Society of the Pacific), ASP Conf. Ser., 322, 419
Whitmore, B. C., Zhang, Q., Leitherer, C., et al. 1999, AJ, 118, 1551
Wilson, C. D., Scoville, N., Madden, S. C., & Charmandaris, V. 2000, ApJ, 542, 120
Zhang, Q., & Fall, S. M. 1999, ApJ, 527, 81